1961

Apparatus for inductive-electromagnetic model studies

Won Ho Kim

Department:

APPARATUS FOR INDUCTIVE-ELECTROMAGNETIC MODEL STUDIES

BY

WON HO KIM

A

THESIS

submitted to the faculty of the

SCHOOL OF MINES AND METALLURGY OF THE UNIVERSITY OF MISSOURI

in partial fulfillment of the work required for the

Degree of

MASTER OF SCIENCE, MINING ENGINEERING MAJOR

Rolla, Missouri

1961

Approved by

H. M. Zern (advisor) G. E. Vaughn

James C. Maxwell Gerald B. Rupert

ABSTRACT

The object of this research is to design, construct and calibrate an apparatus suitable for electromagnetic model studies. A portion of the thesis is devoted to general review and theoretical consideration of electromagnetic prospecting.

Theoretical analysis of electromagnetic survey data by mathematical methods can only be carried out for simple idealized subsurface conditions. Because of the difficulties of theoretical solutions, in contrast to the simplicity of the conditions of similitude in electromagnetic exploration, a model experiment offers a very useful means of studying and comparing the response of naturally occuring conducting mineral bodies.

An apparatus suitable for inductive-electromagnetic model studies with which an extensive study of the electromagnetic response of various kinds of geometric shapes of models can be carried out has been designed. The apparatus is designed to give a linear dimension scale factor of 500 and to use exciting frequency in the model system of 500 cycles per second which gives a frequency scale factor of 2. Aluminum conductors in the model correspond to earth conductors with resistivity of 1.3 ohm-cm.

In the described system, two small coils at a fixed distance apart, one acting as source and the other as receiving coil, are moved over a conductive material. The resulting field in the receiving coil is compared in amplitude and phase angle with the field in the transmitting coil. Results obtained from the model experiment were plotted as curves which show the relationship of amplitude ratio and relative

phase angle with respect to position of the conductive material, and the response curves are directly applicable to interpretation of the field results.

ACKNOWLEDGEMENTS

The author wishes to express his sincere appreciation to Dr. Hughes A. Zenor, professor of Geophysics in the department of Geology, Professor George E. Vaughn, assistant professor of Petroleum Engineering in the department of Mining Engineering, Professor George McPherson, associate professor in the department of Electrical Engineering, Missouri School of Mines and Metallurgy, and Mr. Rudolph A. Black, formerly associate professor of Geophysics in the department of Mining Engineering, Missouri School of Mines and Metallurgy, for their invaluable guidance, advice or for criticism of the manuscript.

TABLE OF CONTENTS

LIST OF FIGURES

LIST OF TABLES

INTRODUCTION

Electromagnetic methods constitute one of the largest and most diversified of the electrical investigations used in geophysical prospecting. In all of these methods, an alternating current is induced in the subsurface material and the characteristics of the magnetic field associated with the flow of this induced current is investigated.

The current is induced in the conductive material by a small transmitting coil equivalent to a magnetic dipole. A receiving coil, also equivalent to a magnetic dipole, in conjunction with its associated circuits measures the vertical component and phase of the resulting magnetic field. Both transmitting and receiving coils remain vertical and at the same elevation, but the distance between and the elevation of the coils may be varied.

The induced voltage in the receiving coil is composed of two components: 1) Voltage from the induced current in the conductive material located below the coils and 2) voltage due to the mutual inductance between receiver and transmitter coils. The phase and amplitude of the resulting field may be measured with a specially designed bridge circuit using a cathode-ray oscilloscope to indicate the nulls.

Several investigators have conducted small scale experiments, but published data available are very limited and not sufficient for widespread use in geophysical interpretation. Slichter[1/] performed experiments using conductive spherical shells placed at a distance from the current exciting loop so that the magnetic field incident at the spheres

---

1/ Numbers in parentheses refer to items listed in the Bibliography of this paper

was essentially uniform and the results were compared to those calculated for such a body. The model was designed to measure only the amplitude of response at six discrete frequencies within the range of 13,000 to 50,000 cycles per second. On the basis of a 50 to 1 frequency scale factor, the equivalent field frequency range was 260 to 1,000 cycles per second. Clark and Mungal (2) studied that particular application of models known as the horizontal loop electromagnetic method. Various-shaped models were placed near the center of a large loop and the total fields were measured at points along a diameter of the loop. An exciting frequency of 50,000 cycles per second was utilized, which corresponds to a frequency scale factor of 100 to 1 on the basis of 500 cycles per second used in field work. Sundberg (3) has determined the field due to currents in rectangular sheets excited by an alternating current in a rectangular loop. More recently, Hedstrom and Parasnis (4) performed model experiments related to electromagnetics with special reference to airborne prospecting. The experiments were made using thin vertical and horizontal conductors of "infinite" extent with coil arrangements utilized in a one transmitter-one receiver unit. The in-phase and quadrature components of the field were measured by the receiver as percent of the amplitude of the normal field at the receiver. These experiments were made using dimensional scales of 1 to 600-2,000 and at frequencies of 500, 880, and 1,500 cycles per second.

A frequency of approximately 500 cycles per second is generally used in electromagnetic field methods. If phase shifts are to be kept negligible or a substantial depth has to be reached, low frequencies in the order of 20-60 cycles per second are preferred. More than one operating frequency may be required when highly conductive layers near the surface are to be penetrated. Electromagnetic methods using

frequencies in the order of tens of kilocycles per second are classed as high frequency methods. These high frequencies lack depth penetration. A frequency range of 200 to 1,000 cycles per second is considered a practical compromise and usually classed as audio-frequency.

Theoretical analysis of electromagnetic survey data obtained by mathematical methods can only be carried out for simple, idealized subsurface conditions. Therefore, most practical interpretations are based on empirical correlation of available electromagnetic and geologic data, or by comparison of field data with the results of electromagnetic model studies. The amount of data on electromagnetic model studies available for widespread use in interpretation of electromagnetic field results is limited.

The purpose of this research problem is to design, construct and calibrate an apparatus suitable for electromagnetic studies with which an extensive study of the electromagnetic response of various models can be carried out. The apparatus to be designed will utilize the horizontal-loop coil configuration with an operating frequency of 500 cycles per second. The dimensional scale factor should be approximately 500 to 1 for reasonable results.

THEORETICAL CONSIDERATION

General

Electromagnetic methods of prospecting are characterized by a measurement in some manner of the magnetic field associated with the flow of current in the subsurface. The methods may be divided generally into two types dependent on the source of the current in the subsurface material; Type 1) The current producing the measured magnetic field is induced by an exciting field from an insulated loop source, or Type 2)

The current producing the measured magnetic field is from a source connected directly to the surface.

Type 1:

The application of primary energy by an insulated loop gives inductive methods a number of advantages over conductive methods. Power can be transferred to the subsurface material without any great loss, particularly in areas of poorly conductive surface beds. Inductive methods offer more efficient results for "sheet-like" deposits; however, the conductive methods are better adapted to massive type structures. Depth penetration control is obtained by use of different frequencies.

Inductively energized methods may be subdivided as follows; 1) Vertical loop method in which the plane of each coil is vertical and 2) Horizontal loop method in which the plane of each coil is horizontal. 1) Vertical-loop Methods: In these methods, vertical current exciting loops are used for energizing the subsurface material. The vertical coil is especially suitable for energizing conductive zones which are vertical or steeply dipping due to the better inductive coupling with such bodies. Using the vertical coil also aids in reducing the effects of interference from highly conductive beds on or near the surface. These advantages are offset by the difficulty of erecting a vertical coil of sufficient size for low frequencies and by creating a weaker magnetic field intensity. The vertical type coils are usually energized by medium to high frequency alternating current so that relatively small size coils may be used, and in order to overcome the lack of energy transfer. The operating frequency must be a compromise since the high frequency will tend to energize any conductive material at shallow depths and thereby not penetrate to the deeper structure.

The vertical transmitting coil is oriented with its plane approximately parallel with the vertical zone to be investigated. The receiving coil is placed parallel to the transmitting coil. The field of the transmitter induces currents on the surface of the conductor which in turn produces a magnetic field surrounding the body. This field combines with the primary field to produce the resultant which is measured in the receiver.

2) Horizontal-loop Methods: In these methods, the subsurface material is energized by the field of a horizontal coil on or above the surface of the ground. The transmitting coil may be linear, rectangular, or circular in construction. In any configuration, the coil should be oriented approximately parallel to the strike of the conductive zone to be investigated and profiled at right angles to the strike.

Receiving equipment will depend on the type of field characteristic to be measured. If only the strike and dip of the elliptical polarization is desired, a simple coil and amplifier with either earphone or a null-detector is required. For the measurement of field intensity without reference to phase changes, a vacuum-tube voltmeter may be used in the output stage of the amplifier, but if intensity and phase in reference to the primary coil current are to be measured, one of various compensator circuits must be used.

Type 2:

In these methods, sometimes known as conductively energized methods, line electrodes are laid out at right angles to the strike of a sursurface structure to be investigated so that maximum distortion of the current lines may occur. Profiles will then be made along these lines at right angles to the strike.

Receiving equipment used in these conductive methods is virtually identical with that in induction methods which was discussed previously for that type. The depth of effective current concentration will be dependent on conductivities of strata involved, and the frequency used.

Interpretation procedures applied to conductive methods vary with the manner in which the resulting magnetic field is measured. If only the direction of the field is measured, the interpretation will be largely qualitative. The direction of the field obtained with a vertical pickup coil or the strike and dip of the ellipse of polarization determined with a coil rotatable along both the horizontal and vertical axis is a function of the following; 1) the normal ground field due to current distribution between the point or line electrodes, 2) the field produced by subsurface current concentration, and 3) the field of the generator leads.

The normal magnetic field as measured by a vertical loop on a line connecting the two current electrodes will be given by:

$$H = I\,(1/r_1 + 1/r_2) \quad \text{- - - - - - - - - - - -} \quad \text{Equation 1 (5)}$$

where, H = resultant normal magnetic field at point P on the line joining the two electrodes, gauss

I = electrode current, ampere in Emu

r_1 and r_2 = distance of point P from the current source and sink, respectively, cm

In interpreting conductive methods, the following corrections are required:

1) Cable leads: The effect of the field of the cable will depend on the position of the receiver with respect to the cable.

2) Topography: The effect of topography may be due to a distortion

of the current lines on the ground surface or a change in relative position between the receiver and conductive body. The effect of distortion of the current lines on the ground surface may be determined by model experiment.

3) Normal Field: A correction for the normal field is necessary in order to determine anomalies caused by subsurface structure.

Depth of Penetration

Since both the frequency of the energizing current and the conductivities of the subsurface limit the effective depth of penetration for electromagnetic methods, many investigators have expressed the relation between these factors. Unlike the use of direct current, the magnitude of alternating current is determined not only by the resistance of the effective circuit but also by the capacitive and inductive reactances, or collectively, the impedance. If a conductor has sufficient cross-section, the inductive reactance to the portion of alternating current flowing near the center will be greater than that near the surface. This is clearly shown by the fact that very high frequency current is confined to the external surface or "skin".

Since the displacement current can be neglected at audio-frequencies used in electromagnetic methods, the depth of penetration of alternating current can be expressed from the laws of electromagnetic wave propagation in terms of velocity and frequency of electromagnetic wave and the resistivity of the medium. The depth at which the surface current density has dropped to 1/e of its value is expressed as follows (6):

$$d = \frac{c}{2\pi}\left(\frac{\rho}{f}\right)^{\frac{1}{2}} \quad \text{- - - - - - - - - - - - - - - - - -} \quad \text{Equation 2}$$

where, d = depth of penetration from surface of the conductor

c = velocity of electromagnetic wave

ρ = resistivity of the conductor

f = frequency of alternating current

Equation 2 shows that the effective depth of penetration squared is directly proportional to the resistivity of the conductor and inversely proportional to the frequency. Since a good conductor at or near the surface will decrease the depth of the current penetration, it is desirable to use low frequencies to obtain sufficient depth investigation.

Response of a Conductor

In regions where the permittivity, permeability and conductivity of a conductor are continuous and an electric charge density together with electric conduction and/or displacement currents, the factor governing the response of the conductor may be found from the solutions of Maxwell's field equations:

$$\nabla \times \underline{E} = -\frac{\partial \underline{B}}{\partial t} \quad \text{Equation 3}$$

$$\nabla \times \underline{H} = \underline{J} + \frac{\partial \underline{D}}{\partial t} \quad \text{Equation 4}$$

$$\nabla \cdot \underline{B} = 0 \quad \text{Equation 5}$$

$$\nabla \cdot \underline{D} = 0 \quad \text{Equation 6}$$

In some high resistive earth materials, it is necessary to consider both the displacement currents and the conduction currents in which the complete equation 4 may be used.

In most earth materials conduction currents are greater than the displacement currents and equation 4 becomes

$$\nabla \times \underline{H} = \underline{J}$$

If the wave motion is sinusoidal of a single frequency, $\frac{\omega}{2\pi}$, one may assume that

$\underline{E} = \underline{E}_o e^{i\omega t}$, electric field vector

$\underline{H} = \underline{H}_o e^{i\omega t}$, magnetic field vector

$\underline{D} = \epsilon \underline{E}$, electric displacement

$\underline{B} = \mu \underline{H}$, magnetic induction

$\underline{J} = \sigma \underline{E}$, current density

- - - - - Equation 7

ϵ, μ, and σ : permittivity, permeability and conductivity of the conductor, respectively.

Placing the relations of equation 7 in equations 3 and 4 yields,

$$\nabla \times \underline{E} = -\frac{\partial \underline{B}}{\partial t} = -\mu \frac{\partial \underline{H}}{\partial t}$$

$$= -\mu (i\omega \underline{H}_o e^{i\omega t})$$

$$= -i\mu\omega \underline{H} \quad \text{- - - - - - - - - - - - Equation 8}$$

and $$\nabla \times \underline{H} = \underline{J} + \frac{\partial \underline{D}}{\partial t} = \sigma \underline{E} + \epsilon \frac{\partial \underline{E}}{\partial t}$$

$$= \sigma \underline{E} + \epsilon (i\omega \underline{E}_o e^{i\omega t})$$

$$= \sigma \underline{E} + i\omega\epsilon \underline{E}$$

$$= (\sigma + i\omega\epsilon)\underline{E} \quad \text{- - - - - - - - - - - - Equation 9}$$

Now taking the curl of $\nabla \times \underline{E}$,

$$\nabla \times (\nabla \times \underline{E}) = \nabla \times (-i\mu\omega \underline{H})$$

$$= -\left[i\mu\omega \nabla \times \underline{H} + (\nabla i\mu\omega) \times \underline{H} \right] \text{- - Equation 10}$$

where gradient $(i\mu\omega) = 0$

$$\nabla \times (\nabla \times \underline{E}) = -i\mu\omega \nabla \times \underline{H}$$

$$\nabla(\nabla \cdot \underline{E}) - \nabla^2 \underline{E} = -i\mu\omega(\sigma + i\omega\epsilon)\underline{E} \quad \text{- - - - - - - - Equation 11}$$

The first term in equation 11 vanishes since the divergence of that electric field is zero,

$$\nabla^2 \underline{E} = i\mu\omega(\sigma + i\omega\epsilon)\underline{E}$$

Similarly,

$$\nabla^2 \underline{H} = i\mu\omega(\sigma + i\omega\epsilon)\underline{H}$$

In cartesian coordinates, these become

$$\frac{\partial^2 E}{\partial x^2} + \frac{\partial^2 E}{\partial y^2} + \frac{\partial^2 E}{\partial z^2} = i\mu\omega(\sigma + i\omega\epsilon)E$$

and

$$\frac{\partial^2 H}{\partial x^2} + \frac{\partial^2 H}{\partial y^2} + \frac{\partial^2 H}{\partial z^2} = i\mu\omega(\sigma + i\omega\epsilon)H \quad \text{- - - - Equation 12}$$

Equation 12 is a general equation for electromagnetic propogation or called the wave equation for harmonic time dependence. Confining to the case in which the waves are propagated along the axis of y, this equation of propagation is

$$\frac{\partial^2 H}{\partial y^2} = -(\mu\epsilon\omega^2 - i\mu\omega\sigma)H \quad \text{- - - - - - - - - - - - Equation 13}$$

$$H = F \text{ Exp.} \left[-i(\mu\omega\sigma - i\mu\epsilon\omega^2)^{\frac{1}{2}} \right] H \quad \text{- - - - Equation 14}$$

where F is constant.

The factor governing the response, the propagation constant of the electromagnetic wave in the medium, is

$$k^2 = (\mu\epsilon\omega^2 - i\mu\omega\sigma) \quad \text{- - - - - - - - - - - - - - - Equation 15}$$

The first term, $\mu\epsilon\omega^2$, is due to displacement currents and the second, $\mu\omega\sigma$, due to conduction currents in the conductor.

Justification of neglecting the displacement current in a conductor in theoretical problems is as follows:

Representative values for μ, ϵ and σ for a non-ferrous conductor are

$$\mu = 4\pi \times 10^{-7} \quad \text{henrys/m}$$

$$\epsilon = 8.8 \times 10^{-12} \quad \text{faradays/m}$$

and in case of aluminum,

$$\sigma = 4 \times 10^{7} \quad \text{mhos/m}$$

Thus, for the effects of displacement current to be 0.1% of conduction current effects, the frequency would have to be approximately 10^{14} cycles per second, as shown by the following examples.

$$0.1 = \frac{\mu\epsilon\omega^2}{\mu\omega\sigma} \times 100$$

$$= \frac{8.8 \times 10^{-12} \times (2 \times 3.14 \times f)}{4 \times 10^{7}}$$

$$f = 7.2 \times 10^{14} \text{ cycles per second}$$

Therefore, considering the above example, displacement current can be neglected in theoretical study of electromagnetic methods used for geophysical investigation.

THEORY OF MODEL SCALING

In the interpretation of results of some methods of geophysical investigation, scale model experiments have been made and used. For experiments applicable to the electromagnetic methods, small scale models are used to simulate ore bodies or subsurface structures. A large reduction in size is made to acommodate models of conductive material. Reduction in size or linear dimension is offset by increasing the conductivities of the various media and/or by increasing exciting frequency. By appropriate scaling, it is possible to simulate the configurations of the lines of force. Results from the model work, despite the fact that the model and full scale sources are far different, are then directly applicable to field conditions.

General Scaling Conditions

The conditions under which a model system may accurately reproduce the geometrical configurations of the lines of force in the full scale system have been developed by many workers from the theory of similitude. The most extensive treatment for the electromagnetic problem has

been published by Sinclair. (7)

Maxwell's differential equations describing any electromagnetic field are linear and permit linear scaling provided such non-linear media as ferromagnetics and ionized fluids are excluded.

As shown previously, displacement currents may be neglected and conductivity assumed constant with respect to field strength and time for most geophysical problems.

Consider a region in which there is a good conducting body surrounded by a poorly conductive rock mass. For such a system, assume an oscillating magnetic dipole located at the origin of a reference frame is generating a magnetic field. It will then be required to determine the conditions which have to be satisfied in a model of this system to

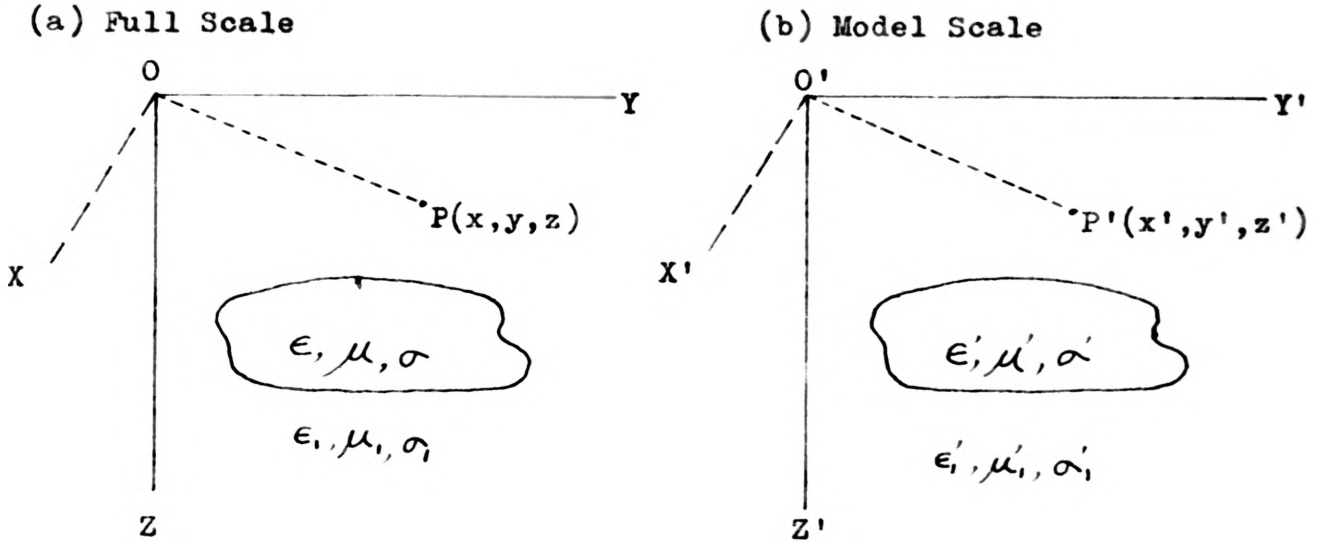

Figure 1a and 1b. Geometrical Distribution of Parameters in Full and Model Scale Systems

simulate configurations of the lines of force.

Using figure 1a and 1b to represent the system, let any point P in the full scale system be located by the rectangular coordinates (x, y, z). Then any point P' of the model is located by the coordinated (x', y', z') in the corresponding model coordinate system. The two coordinate systems are related by the transformations:

$$\left.\begin{aligned} x &= Sx' \\ y &= Sy' \\ z &= Sz' \end{aligned}\right\} \text{ - - - - - - - - - - - - - - - - - - Equation 16}^{2/}$$

where S is the linear scale factor.

The conditions imposed by equation 16 represent the principal requirements for a "linear" model. The coordinates (x, y, z) and (x', y', z') are measured in units of length, and the same unit of length must be used for both systems.

Since there are other parameters which require scaling in an absolute electromagnetic model, the following conditions must be added to those of equation 16.

$$t = gt' \text{ - Equation 17}$$

$$\underline{E}(x,y,z,t) = m\underline{E}'(x',y',z',t') \text{ - - - - - - - - - Equation 18}$$

$$\underline{H}(x,y,z,t) = n\underline{H}'(x',y',z',t') \text{ - - - - - - - - - Equation 19}$$

$$\sigma(x,y,z) = p\sigma'(k',y',z') \text{ - - - - - - - - - - Equation 20}$$

g = scale factor for time

$\frac{1}{g}$ = scale factor for frequency

m = scale factor for electric intensity

n = scale factor for magnetic intensity

p = scale factor for conductivity (derived on page 17)

2/ Primed quantities refer to model system and all other refer to full scale system.

When the scale factors (ζ,g,m,n) are known quantities, equations 16, 17, 18, 19 and 20 represent the conditions which must be satisfied in the model and the relationships between all other electromagnetic quantities for the two systems will be fixed. Since the fields in both systems must satisfy the Maxwell's equations (Equations 3, 4, 5, 6), the relationship between the various quantities may be determined as follows:

Full scale ---

$$\text{Curl } \underline{H}(x,y,z,t) = \sigma(x,y,z,) \underline{E}(x,y,z,t) + \epsilon(x,y,z)\frac{\partial \underline{E}}{\partial t}(x,y,z,t) \qquad \text{Equation 21}$$

$$\text{Curl } \underline{E}(x,y,z,t) = -\mu(x,y,z)\frac{\partial}{\partial t}\left[\underline{H}(x,y,z,t)\right] - - \qquad \text{Equation 22}$$

Model scale ---

$$\text{Curl}' \ \underline{H}'(x',y',z',t') = \sigma'(x',y',z')\underline{E}'(x',y',z',t') + \epsilon'(x',y',z')\frac{\partial \underline{E}'}{\partial t'}(x',y',z',t') \quad - - - - - - - \text{ Equation 23}$$

$$\text{Curl}' \ \underline{E}'(x',y',z',t') = -\mu'(x',y',z')\frac{\partial}{\partial t'}\left[\underline{H}'(x',y',z',t')\right] \qquad \text{Equation 24}$$

The symbol "Curl'" means that the differentiations are to be performed in the primed coordinate system; for example, the component of Curl' $\underline{H}'$ directed parallel to the x' axis is

$$\text{Curl}' \ H' = \begin{vmatrix} \underline{i} & \underline{j} & \underline{k} \\ \frac{\partial}{\partial x'} & \frac{\partial}{\partial y'} & \frac{\partial}{\partial z'} \\ H'_{x'} & H'_{y'} & H'_{z'} \end{vmatrix}$$

$$\text{Curl}'_{x'} \ H' = \frac{\partial H'_{z'}}{\partial y'} - \frac{\partial H'_{y'}}{\partial z'}$$

where $H'_{z'}$ is the component of Curl' $\underline{H}'$ which is directed parallel to the z' axis, etc.

If the model system is an accurate simulation of the full-scale system, then inserting the transformations relating model quantities to

full-scale quantities should transform equations 23 and 24 into equations 16, 17, 18 and 19 into equations 23 and 24 and comparing the results which relate the parameters ϵ, σ, μ of the two systems as follows:

By equation 16,

$$\frac{d H_z'}{dy'} = \frac{d H_z'}{dy} \frac{dy}{dy'} = S \frac{dH_z'}{dy} \quad \text{- - - - - - - -} \quad \text{Equation 25}$$

and similarly for the other components.

Hence by equation 19,

$$\text{Curl}'\underline{H}' = S \text{ Curl } \underline{H}' = (S/n) \text{ Curl } \underline{H} \quad \text{- - - - -} \quad \text{Equation 26}$$

and similarly,

$$\text{Curl}'\underline{E}' = (S/m) \text{ Curl } \underline{E} \quad \text{- - - - - - - - - - - - -} \quad \text{Equation 27}$$

By equation 17,

$$t = gt'$$

$$\frac{\partial}{\partial t} = \frac{1}{g} \frac{\partial}{\partial t'}, \quad \frac{\partial}{\partial t'} = g \frac{\partial}{\partial t}$$

Then, $$\frac{\partial \underline{E}'}{\partial t'} = g \frac{\partial \underline{E}'}{\partial t} = \frac{g}{m} \frac{\partial \underline{E}}{\partial t} \quad \text{- - - - - - - - - - - -} \quad \text{Equation 28}$$

Substituting equations 18, 19, 26, 27 and 28 into equations 23 and 24:

$$\frac{S}{n} \text{ Curl } \underline{H}(x,y,z,t) = \sigma'(x',y',z') \frac{\underline{E}}{m}(x,y,z,t) +$$

$$\frac{g}{m} \epsilon'(x',y',z') \frac{\partial \xi}{\partial t}(x,y,z,t) \quad \text{- - - - - - - - - -} \quad \text{Equation 29}$$

$$\frac{S}{m} \text{ Curl } \underline{E}(x,y,z,t) = -\mu'(x',y',z') \frac{g}{n} \frac{\partial}{\partial t} \left[\underline{H}(x,y,z,t) \right] \quad \text{Equation 30}$$

These two equations must be identical with equations 21 and 22 for accurate simulation. Hence,

$$\frac{n}{Sm} \sigma'(x',y',z') = \sigma(x,y,z) \quad \text{- - - - - - - - - - -} \quad \text{Equation 31}$$

$$\frac{ng}{Sm} \epsilon'(x',y',z') = \epsilon(x,y,z) \quad \text{- - - - - - - - - - -} \quad \text{Equation 32}$$

$$\frac{mg}{Sn} \mu'(x',y',z') = \mu(x,y,z) \quad \text{- - - - - - - - - - -} \quad \text{Equation 33}$$

The interpretation of these equations requires the conductivity at the point P'(x', y', z') in the model to be equal to (Sm/n) times the conductivity at the corresponding point P(x, y, z) in full scale system. Other equations are interpreted similarly. Therefore,

$$\sigma' = \frac{Sm}{n}\sigma \quad \text{- -} \quad \text{Equation 34}$$

$$\epsilon' = \frac{Sm}{ng}\epsilon \quad \text{- - - - - - - - - - - - - - - - - - - -} \quad \text{Equation 35}$$

$$\mu' = \frac{Sn}{mg}\mu \quad \text{- - - - - - - - - - - - - - - - - - - -} \quad \text{Equation 36}$$

These three equations represent the conditions which must be satisfied by the medium so that a model can be constructed for which the simulation is correct.

Simplification of Scaling Condition

Further simplification of scaling not given by Sinclair (7), is possible if the displacement current is neglected as discussed previously. Then, by neglecting the displacement current, equations 29 and 30 may be rewritten as follows:

$$\frac{S}{n}\,\text{Curl}\,\underline{H}(x,y,z,t) = \sigma'(x',y',z')\frac{\underline{E}}{m}(x,y,z,t) \quad \text{- -} \quad \text{Equation 37}$$

$$\frac{S}{m}\,\text{Curl}\,\underline{E}(x,y,z,t) = -\mu'(x',y',z')\frac{g}{n}\frac{\partial}{\partial t}\{\underline{H}(x,y,z,t)\} \quad \text{Equation 38}$$

Comparing equations 37 and 38 with equations 21 and 22 shows that the following relationships must hold:

$$\frac{n}{Sm}\sigma'(x',y',z') = \sigma(x,y,z) \quad \text{- - - - - - - - - -} \quad \text{Equation 39}$$

$$\frac{mg}{Sn}\mu'(x',y',z') = \mu(x,y,z) \quad \text{- - - - - - - - - -} \quad \text{Equation 40}$$

Thus, the restricting equations for m, n, g and S have been reduced from three as in the previous case to two.

For any arbitrary choice of four conditions (S, g, m, n) it is theoretically possible to construct an exact model to simulate a given full scale system. However, in practice, there are certain restrictions on the choice of scale factors which results from the limited ranges of μ, σ, and ϵ available in media which can be used for model. For example, when ferromagnetic media are excluded from the model it is evident that the permeability of the model media cannot differ appreciably from the permeability for free space, therefore for all media,

$$\mu'(x',y',z') = \mu(x,y,z)$$
$$= 4\pi \times 10^{-7} \text{ henry/meter}$$

and it follows from equation 36 that:

$$\frac{Sn}{mg} = 1$$

or

$$\frac{n}{Sm} = \frac{g}{S^2} \quad \text{- -} \quad \text{Equation 41}$$

By substituting the relationship in equation 41 into equation 39, the following simplified model scaling equation may be written:

$$\sigma'(x',y',z') = \frac{S^2}{g}\sigma(x,y,z)$$

if $\sigma = p\sigma'$ where p is a scale factor for conductivity,

$$p = g/S^2$$

or

$$\frac{pS^2}{g} = 1 = \text{Constant} \quad \text{- - - - - - - - - - - - -} \quad \text{Equation 42}$$

Scaling Condition by Electrodynamic Similitude

When the theory of similitude is applied to a problem, it is customary to express the conditions of the experiment in terms of a dimensionless parameter. Thus, if this parameter is kept constant, the condition may be varied within the experiment, and the results which

apply to a small scale experiment may also be applied to a full scale operation.

Stratton (8) has shown that the parameter Θ for electrodynamic similitude is

$$\Theta^2 = (\mu\omega\sigma - i\mu\epsilon\omega^2)\ell^2$$

$$\Theta = (\mu\omega\sigma - i\mu\epsilon\omega^2)^{\frac{1}{2}}\ell \text{ - - - - - - - - - - - - - Equation 43}$$

As shown previously, $\mu\epsilon\omega^2$ is negligible when compared to $\mu\omega\sigma$. Similitude requires that Θ remains invariant with changes in scale. For the model experiment, then, it is necessary that

$$\Theta = (\mu\omega\sigma)^{\frac{1}{2}}\ell = \text{Constant - - - - - - - - - - - - Equation 44}$$

It may be noted from equation 44 that the parameter Θ is independent of magnetic field intensity or electric field intensity since their magnitudes depend only on the available power.

Equation 44 may be rewritten in the following form to show the relation between model and full scale parameters.

$$(\mu_o\omega_o\sigma_o)^{\frac{1}{2}}\ell_o = (\mu_m\omega_m\sigma_m)^{\frac{1}{2}}\ell_m = \text{Constant}$$

or

$$\frac{\mu_o f_o \ell_o^2}{\rho_o} = \frac{\mu_m f_m \ell_m^2}{\rho_m} = \text{Constant - - - - - - - Equation 45}$$

where, ℓ: pertinent linear dimensions

$f = \frac{\omega}{2\pi}$: frequency of transmitted electromagnetic wave

$\rho = \frac{1}{\sigma}$: electrical resistivity

μ: magnetic permeability

Subscripts "o" and "m" denote the field and the model parameters, respectively.

If μ_o can be considered equal to μ_m as for non-magnetic materials, and the previously defined scale factors

$$\left.\begin{aligned} \frac{\ell_o}{\ell_m} &= S \\ \frac{\mu_o}{\mu_m} &= 1 \\ \frac{f_o}{f_m} &= \frac{1}{g} \\ \frac{\rho_o}{\rho_m} &= \frac{1}{p} \end{aligned}\right\} \text{ - Equation 46}$$

are substituted into equation 45, the following relation identical to equation 42, is obtained:

$$\frac{(\mu_m)\ (f_m/g)\ (\ell_m S)^2}{(\rho_m/p)} = \frac{\mu_m f_m \ell_m^2}{\rho_m}$$

$$\frac{S^2 p}{g} = 1 \text{ - Equation 47}$$

It is seen from equation 45 that if ℓ_o is decreased by a factor of 200(i.e. S = 200) an increase of 4×10^4 in either frequency and/or conductivity in the model is required if the equation is to remain equivalent.

Since a frequency of 500 cycles per second in the model represents a frequency of 1000 cycles per second at field condition, the apparatus described is designed to give a frequency scale factor of 2(i.e. 1/g = 2) and a linear scale factor of 500(i.e. S = 500). Substituting these values into equation 47, the conductivity scale factor is obtained as follows:

$$\frac{S^2 p}{g} = \frac{(500)^2 p}{\frac{1}{2}}$$

or

$$p = 2 \times 10^{-6}$$

Therefore, the conductivity of the model material will be 5×10^5 times as great as the earth material.

DESCRIPTION OF MODEL EQUIPMENT

Figure 2 shows the general block diagram of the equipment designed to be used in extensive study of models by electromagnetic methods. The following components will be discussed in detail:

1) Signal Generator
2) Preamplifier
3) Cathode-ray Oscilloscope
4) Transmitting and Receiving Coils
5) Supporting Coil Frame
6) Phase Shifter
7) Fixed Phaser
8) Balancer

All components excluding the signal generator, preamplifier, and oscilloscope were specially designed and constructed for the purpose of this electromagnetic model study. Description of the design, construction and operation of each component used in the model equipment is as follows:

1) Signal Generator:

The signal generator used in the model system was a Heathkit model AG-9A audio generator. The circuit diagram of this instrument consists of four main parts: 1) power supply, 2) oscillator, 3) attenuator, and 4) metering circuit. The generator is designed to operate from a 105-125 volt, 50-60 cycles, 40 watt source. Manufacturer's specifications indicate a frequency accuracy of $\pm$ 5% cycles per second over its full range coverage of 1 cycle to 100 KC and output distortion of less than 0.1%. Laboratory checks with a cathode ray oscilloscope showed negligible distortion of the sine wave up to output levels of

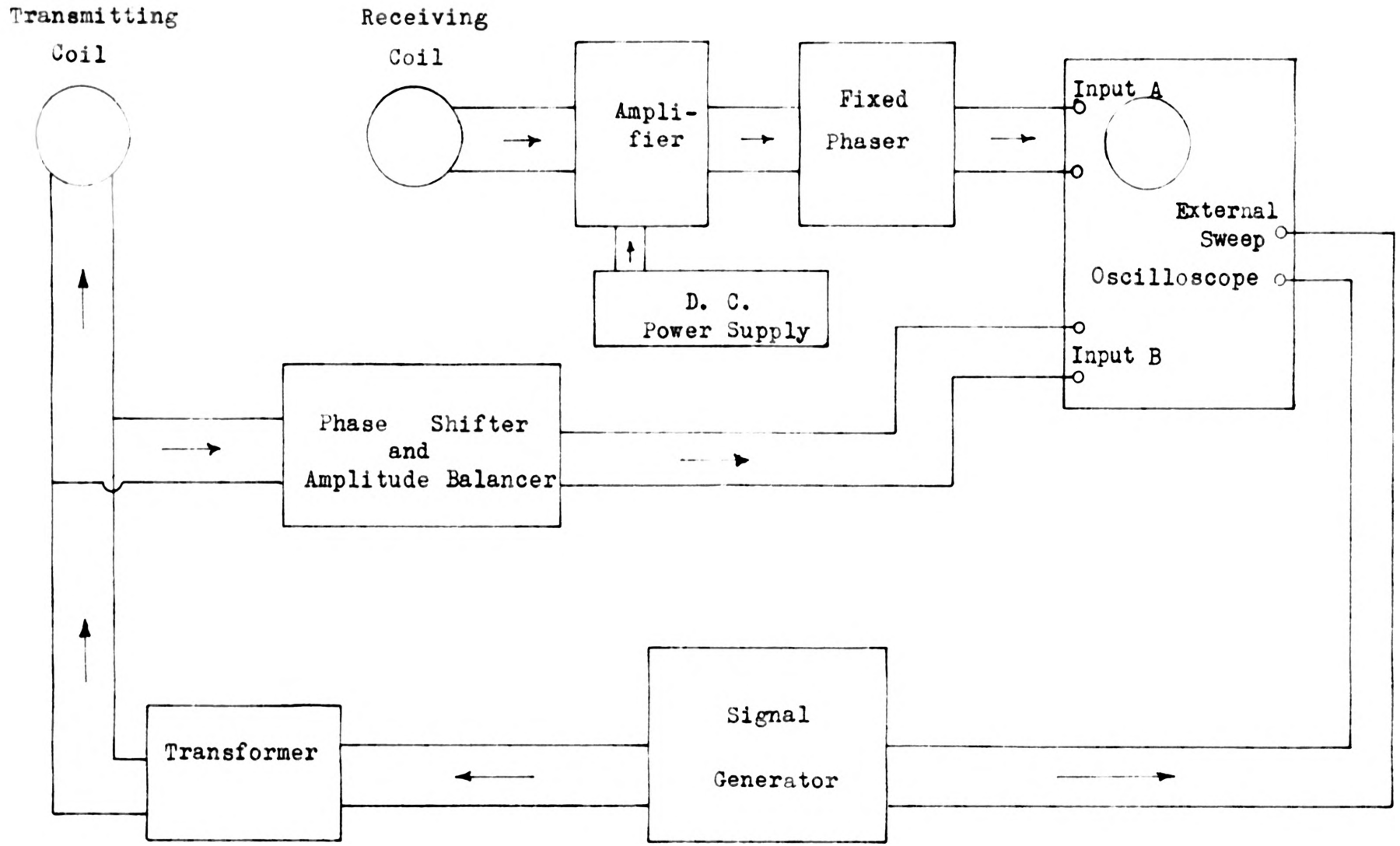

Figure 2. Block Diagram of Model Study Equipment

(a) (b)

Figure 3. (a) Preamplifier and (b) Signal Generator

7.5 volts and only slight distortion above this level.

2) Preamplifier:

The preamplifier is a Tektronix type 122 amplifier. This amplifier is a compact, R. C. coupled, three stage, battery-operated amplifier which is designed primarily to extend the sensitivity of the Tektronix oscilloscope. However, the Tektronix type 122 preamplifier may be put to general use as an amplifier by grounding the input to VIB (see figure 4) and connecting the signal to be amplified to VIA.

At maximum bandwidth setting, frequency response is essentially flat at 3-db points between lower and upper frequency limits of 0.16 cycles and 40 kilocycles. A maximum output of 20 volts, peak to peak, is available without appreciable distortion of amplitude linearity. At a gain of 1,000 times (or high gain) and at a gain setting of 100 times (or low gain), the maximum undistorted output is 10 volts. Maximum input level of the amplifier is 0.02 volts, peak to peak, at the high gain setting and 0.10 volts at the low gain setting.

The amplifier is designed to select upper cutoff frequencies at 40 kc, 10 kc, 250 cycles, and 50 cycles, and cutoff frequencies at 0.2 cycles, 0.8 cycles, and 80 cycles.

Since the optimum frequency of 500 cycles per second was selected as the design frequency for the electromagnetic model apparatus, satisfactory upper and lower 3-db points were selected at 1 kc and 80 cycles per second, respectively.

3) Cathode-ray Oscilloscope:

The oscilloscope used in the experimental system is a Tektronix type 535 cathode-ray oscilloscope with an associated type 53/54d plug-in unit (see figure 5).

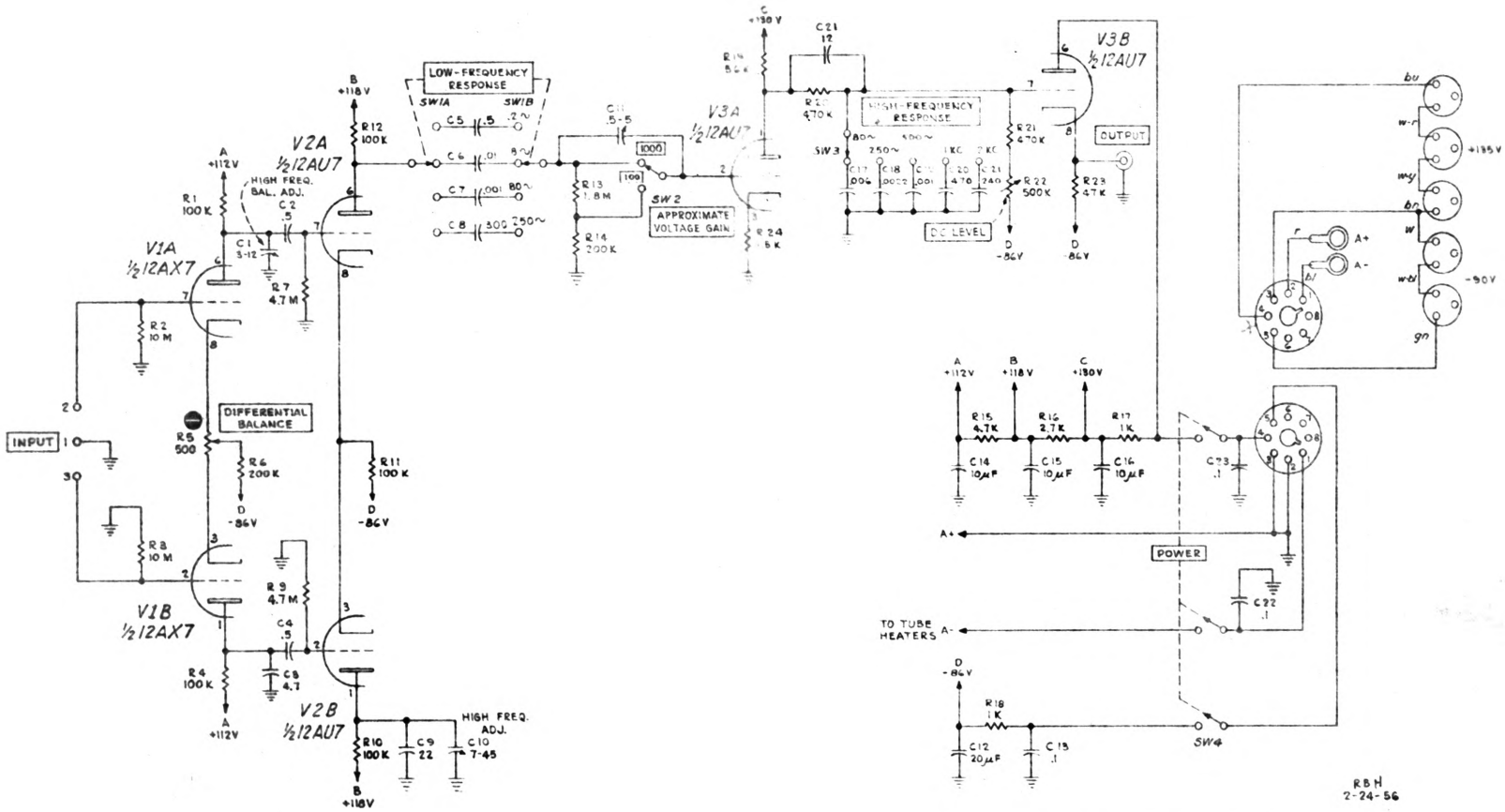

TYPE 122 LOW-LEVEL PREAMPLIFIER

Figure 4. Circuit Diagram of Preamplifier

The type 535 oscilloscope was designed for general laboratory use and is equipped with accurately calibrated sweeps and vertical-deflection sensitivities which permit quantitative time and amplitude measurements to be made with accuracies comparable to that of indicating meters. Accurately delayed, triggered sweeps make it possible to select and observe minute portions of voltage waves.

The type 53/54 plug-in unit is used as a preamplifier with the type 535 oscilloscope. Either of two separate signal inputs can be selected independently or simultaneously. Simultaneous input permits mixing of two signals so that the difference may be fed to the main amplifier of the scope. This feature of the plug-in unit was used in the model equipment to indicate the voltage nulls in the receiver coil as related to the impressed voltage in the transmitter coil.

4) Transmitting and Receiving Coils:

The transmitting coil consists of 200 turns of No. 32 enamel copper wire which is wound on a circular plastic spool of $\frac{1}{2}$ inch diameter. The leads from the transmitting coil are connected to the secondary winding of the transformer and to the input of the phase shifter circuit as shown in figure 7.

The receiving coil consists of 600 turns of No. 36 enamel copper wire which is wound on a circular plastic spool of 3/4 inch diameter. The 0.1 μf capacitor connected across the receiving coil functions to eliminate undersirable high frequency noise which may be derived from outside sources, such as the transmitter of a local radio station. The receiving coil is connected to the input of the amplifier where the voltage induced in the coil is amplified at a gain of 100 times. Two conductor, shielded intercom cables were used as interconnecting leads for both coils.

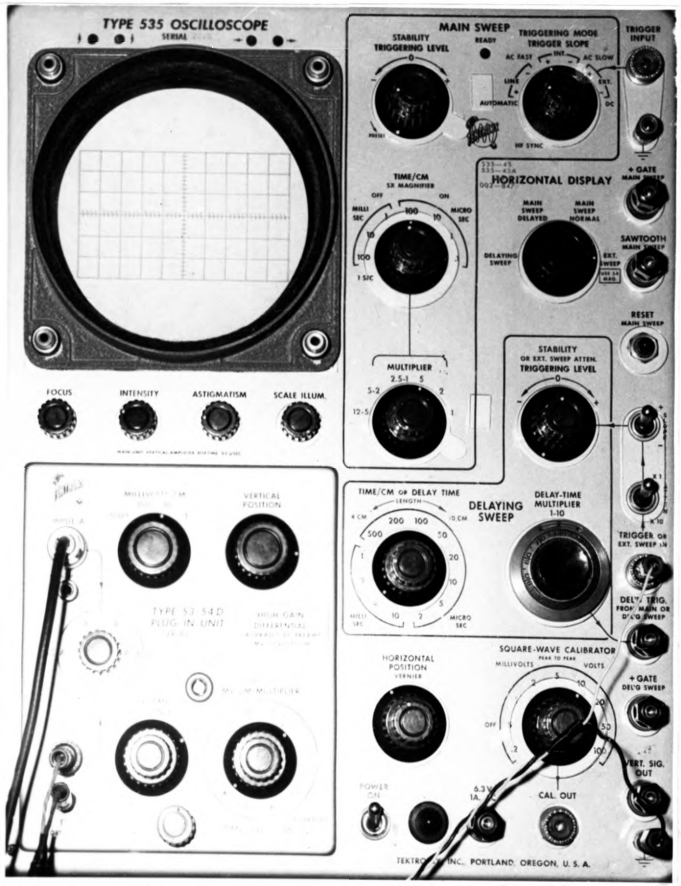

Figure 5. Cathode-ray Oscilloscope

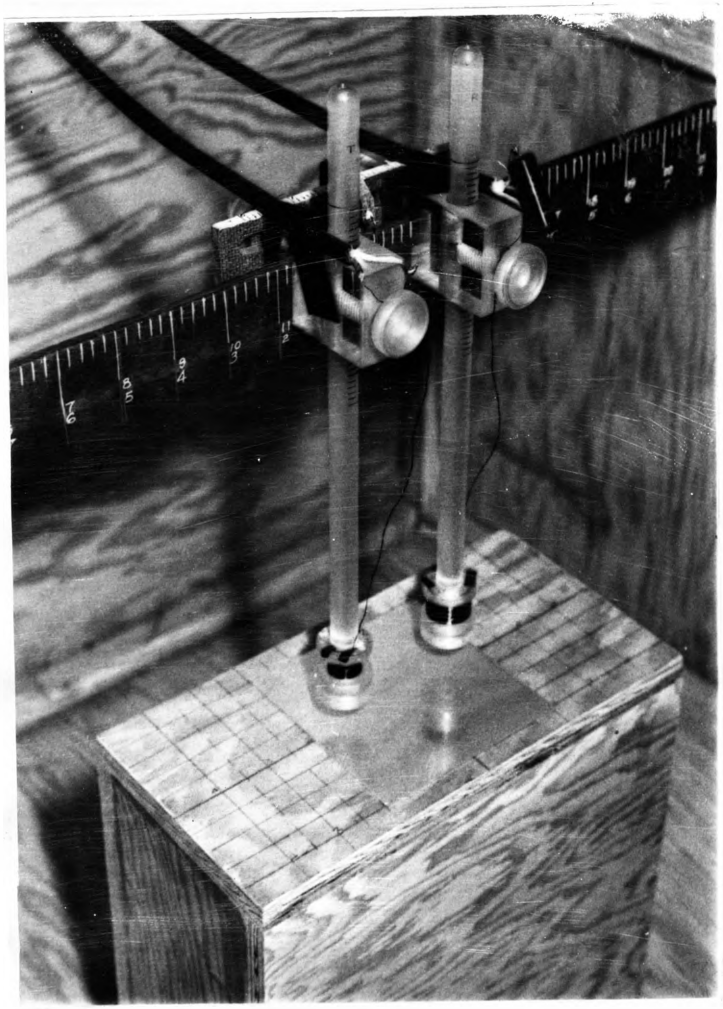

Figure 6. Supporting Coil Frame

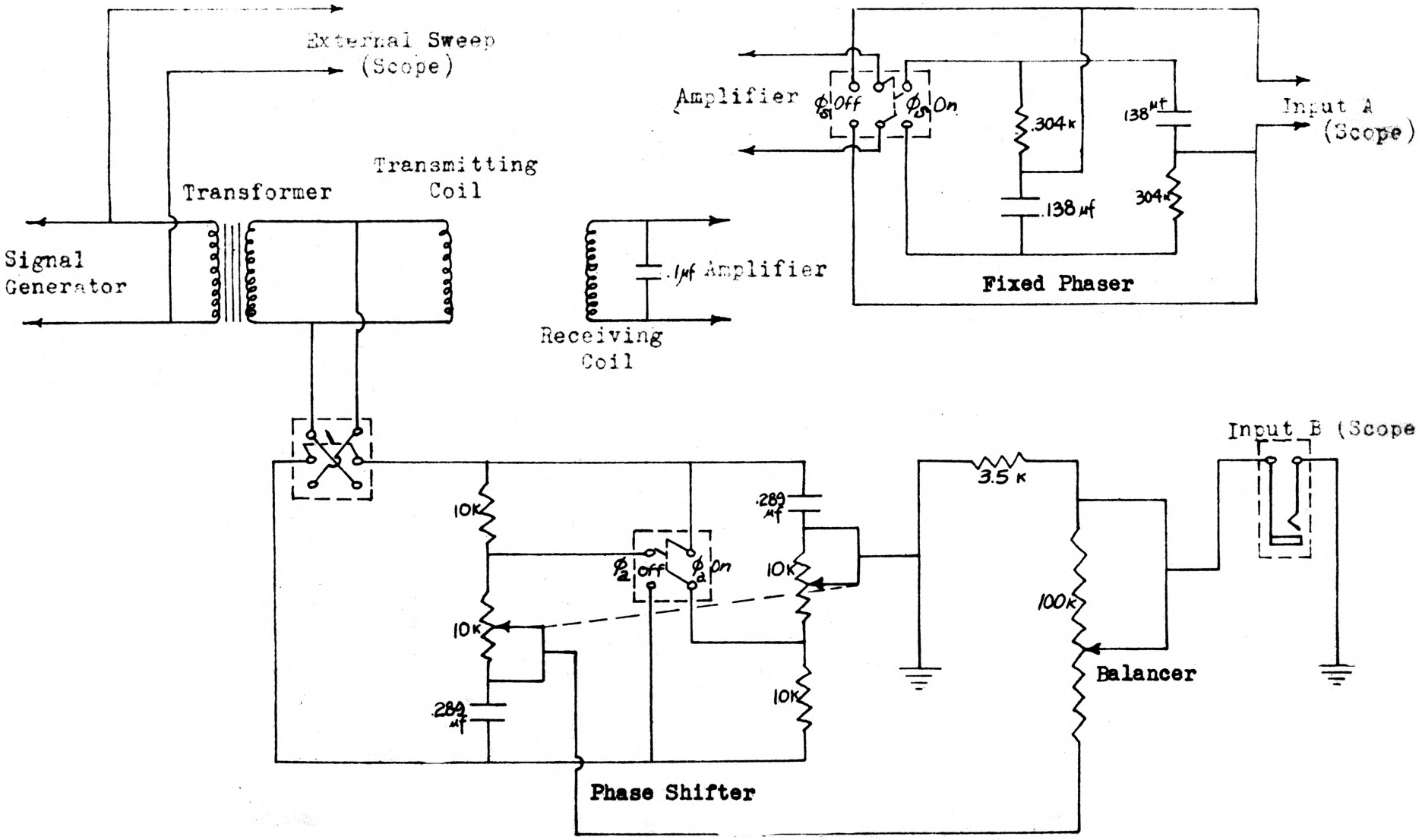

Figure 7. Schematic Diagram of Model Study Equipment

5) Supporting Coil Frame:

The frame supporting the coils was constructed using non-conductive material throughout to prevent any distortion of the magnetic field under study. Also, the frame was rigid enough so that no inconsistancy was introduced due to flexibility while measurements were being made. The model and coil system are contained within a 3 ft. x 3 ft. x 2 ft. box made of $\frac{1}{2}$ inch plywood using Weldwood glue instead of nails or screws. A 6 in. x 10 in. x 10 in. specimen stand used to support the models was also constructed in the same manner.

The coil attachments which support the plastic columns to which the coil spools are fastened are grooved in such a manner to allow sliding horizontally along the rigid cross span as shown in figure 6. The span is made of $\frac{1}{4}$ inch tempered masonite and marked with 0.2 inch graduations. The plastic columns supporting the coil spools are fastened to the coil attachments with plastic set screws and are marked with 0.1 inch graduations. These graduations indicate the vertical distance between the bottom of the model and the horizontal plane through the centers of the coils.

6) Phase Shifter:

As shown in figure 7, the phase shifter is composed of two branches one composed of a 10 K resistor, 10 K potentiometer, and 0.289 μf capacitor in series, and the other composed of identical components connected in reverse order. The potentiometers used in the phase shifter circuit are two General Radio Company Type 977-N potentiometers having the following characteristics: independent linearity, $\pm$ 0.2%; temperature coefficient of resistivity, 0.002%; standard resistance tolerance, $\pm$ 2%; and mechanical rotation, 320 degrees.

The two 10 K fixed resistors may be switched in or out of the circuit by throwing to the ON or OFF position, respectively. With the switch in the OFF position, the phase shifter can measure changes in phase angle from 0 to 167.4 degrees, and in the ON position an additional range of phase angle from 167.4 to 173.7 degrees can be measured.

7) Fixed Phaser:

The fixed phaser is similar to the phase shifter described in the previous section with the exception that the change of phase angle is fixed at 15 degrees. The two branches are each composed of a 305 ohm resistor in series with a 0.138 μf capacitor and connected in reverse.

The phase angle change of 15 degrees was calculated using equation 50 as follows:

$$\phi = 180^\circ - 2\tan^{-1}\left(\frac{X_c}{R}\right)$$

where, $$X_c = \frac{1}{2\pi fc} = \frac{1}{2x3.14x500x0.138x10^{-6}} = 2.303K$$

$$R = .304K$$

Thus, $$\phi = 180^\circ - 2\tan^{-1}\left(\frac{2.303}{0.304}\right) = 15^\circ$$

The purpose of using the fixed phaser is to shift the phase angle of the receiving coil so that the phase shifter can operate in its relatively sensitive range above 150 degrees. It was noted that this phase shift of 15 degrees does not alter the shapes of the response curves since relative changes in phase angles remain the same.

8) Balancer:

The 10 K potentiometer as shown in figure 7 is called the "Balancer". It is a Burg ten turn precision potentiometer with a linearity of 0.5% and mechanical and electrical rotation of 3600 degrees. Its function in

the circuit is to balance out the voltage output from the phase shifter with an amplified voltage from the receiving coil by using a cathode-ray oscilloscope to indicate proper balance.

CALIBRATION

Operation of the model equipment requires that the phase shifter and balancer be calibrated. Each component must be calibrated independently, and considerable time is involved to maintain the required accuracy. The phase shifter is calibrated to show the phase shift angle indicated at various instrument dial settings. Calibration of the balancer shows the relation of peak to peak output voltage at various input voltages to instrument dial settings. The only equipment required for calibration of both components is a cathode-ray oscilloscope and a signal generator equipped with a step down transformer as described later.

Phase Shifter

Calibration was first done by calculation based on analysis of the phase shifter circuit and then the results were spot checked by means of "Lissajous figures" on a cathode-ray oscilloscope.

Circuit Analysis:

The phase shifter is essentially composed of two branches; each composed of an identical resistor and capacitor in series and the two connected in reverse as shown in figure 8. When connected in this manner, the potential drop from a to b will be the same across either branch.

For analysis, let the impressed emf between a and b and c and d be V_{ab} and V_{cd}, respectively, and the frequency f cycles per second. Since the potential drop is the same across either branch, it may be made

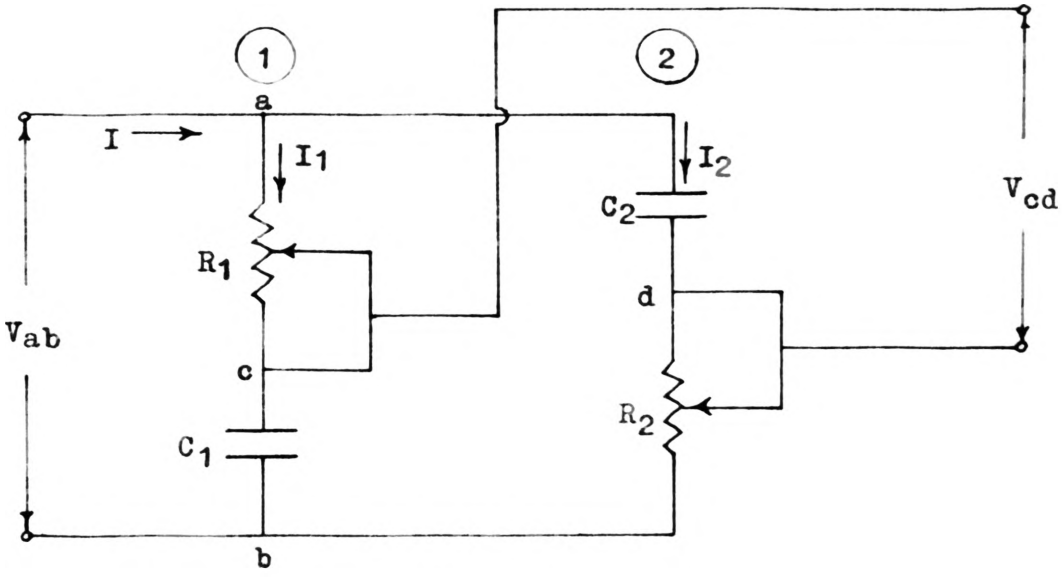

Figure 8. Simplified Schematic Diagram of Phase Shifter

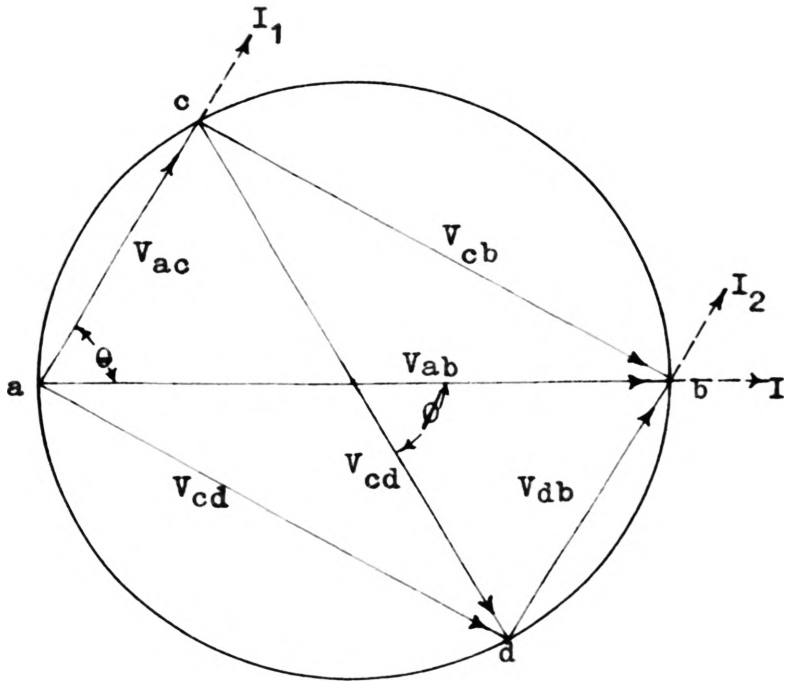

Figure 9. Vectorial Analysis of Phase Shifter

common to the vector triangles for the two branches and is represented by the line ab in figure 9. The triangle acb is the potential triangle for branch 1, adb the potential triangle for branch 2. These triangles are inscribed in a circle, the diameter of which is the potential drop ab and each is a right triangle. The resulting phase angle between the input, V_{ab}, and the output, V_{cd}, of phase shifter is indicated as ϕ in figure 9.

Since the components in each branch are the same; i.e. $R_1 = R_2 = R$, and $C_1 = C_2 = C$, and $I_1 = I_2 = I'$, the following relations may be written:

$$\theta = \tan^{-1} (V_{cb}/V_{ac})$$

$$= \tan^{-1} (V_{ad}/V_{db})$$

$$= \tan^{-1} (I'X_c/I'R)$$

$$= \tan^{-1} (X_c/R) \quad \text{- - - - - - - - - - - - - - -} \quad \text{Equation 48}$$

where, $X_c = 1/2\pi fC$ = Capacitive reactance

R = Resistance

C = Capacitance

Since acbd is inscribed in a circle, it is seen that

$$2\theta + \phi = 180^\circ$$

or $$\phi = 180^\circ - 2\theta \quad \text{- - - - - - - - - - - - - - - - -} \quad \text{Equation 49}$$

Substituting equation 48 into equation 49,

$$\phi = 180^\circ - 2\tan^{-1} (X_c/R) \quad \text{- - - - - - - - - - -} \quad \text{Equation 50}$$

or rewritting equation 50 in a different form,

$$R = X_c \cot \left(\frac{180^\circ - \phi}{2} \right)$$

or $$R = X_c \cot (90^\circ - \phi/2) \quad \text{- - - - - - - - - - - - -} \quad \text{Equation 51}$$

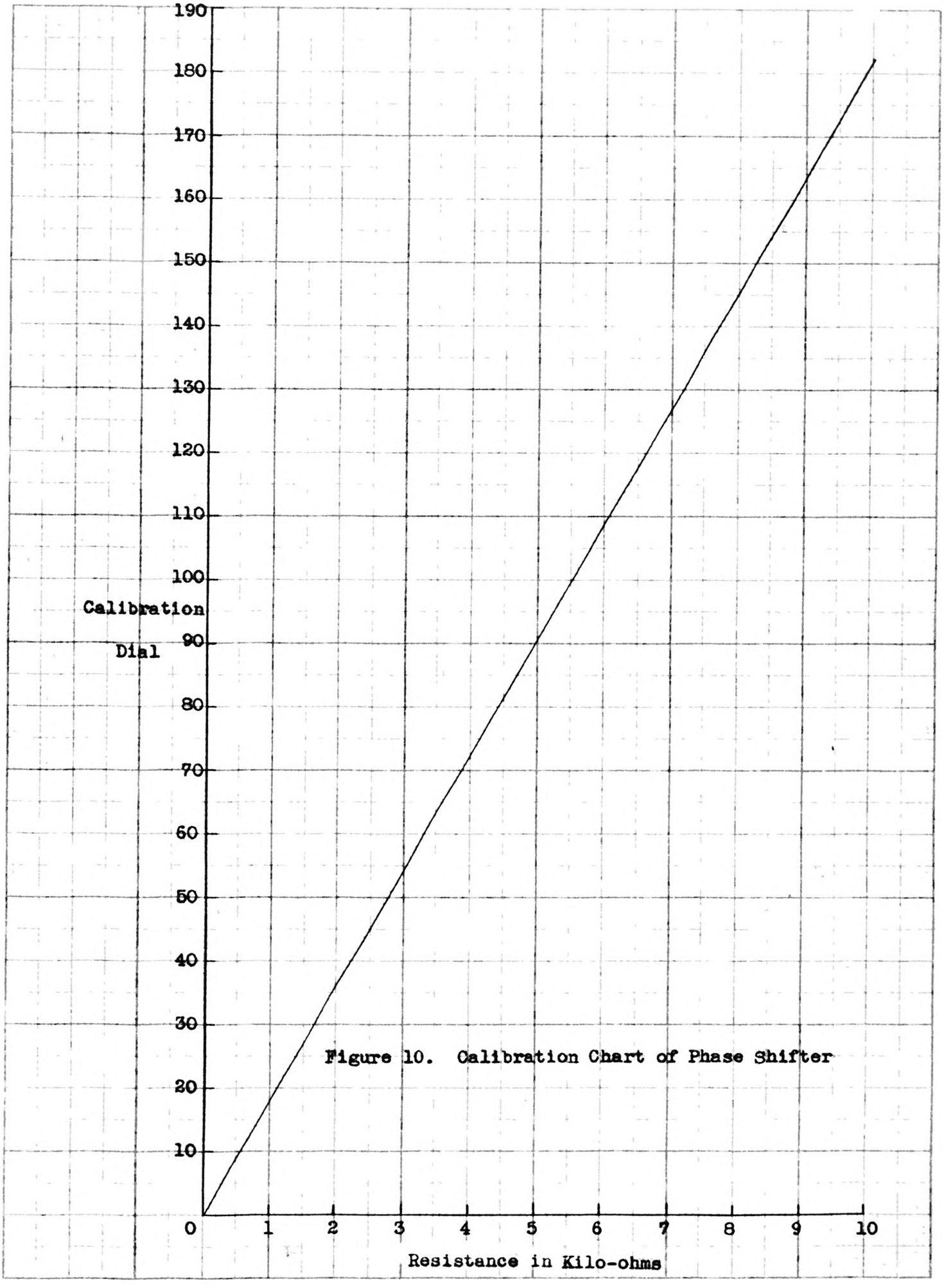

Figure 10. Calibration Chart of Phase Shifter

Since X_c is a fixed value, values of R are obtained by substituting various values of phase angle into equation 51. With the switch ϕ_a in the "OFF" position, the phase shifter can measure a phase angle of 0-167.4° and with it in the "ON" position a phase angle of 167.4° -173.7° giving an additional 6.3° range. Equation 50 shows that 180° of phase angle can only be obtained when R values approach infinity; however, the range of 0°-173.7° is sufficient for model studies.

Since the potentiometers used in the phase shifter circuit offer high linearity, readings of the calibration dial on the phase shifter are directly proportional to values of the potentiometers. The calibration chart shown in figure 10 is made by applying the linear relationship between the calibration dial and potentiometer value.

Readings of the calibration dial of the phase shifter which correspond to the values of R calculated using the relation in equation 51 for different phase angles are shown in the calibration chart in Table 1, and the corresponding phase angles are marked as graduations on the instrument panel.

Lissajous Figure:

The cathode-ray oscilloscope offers a simple way of determining the phase angle. If two sinusoidal voltages are applied respectively to the horizontal and vertical deflection plates of a cathode-ray oscilloscope, the resulting pattern, known as a "Lissajous figure", may be used to determine the phase angle.

Consider the two sinusoidal voltages V_{ab} and V_{cd} as shown in figure 8, being applied to the horizontal and vertical deflection plates respectively of a cathode-ray oscilloscope. Since both voltages vary sinusoidally and differ by a phase angle ϕ, the deflections along the

y-axis and x-axis, figure 11, are as follows:

$$y = B \sin(\omega t) \quad \text{- - - - - - - - - - - - - - - - - -} \quad \text{Equation 52}$$

$$x = A \sin(\omega t - \phi) \quad \text{- - - - - - - - - - - - - - - - -} \quad \text{Equation 53}$$

where, y = deflection along the y-axis

x = deflection along the x-axis

ωt = angle through which sine wave has progressed

ω = $2\pi f$

A = maximum or peak value of sinusoidal voltage applied to the horizontal deflection plates

B = maximum or peak value of sinusoidal voltage applied to the vertical deflection plates

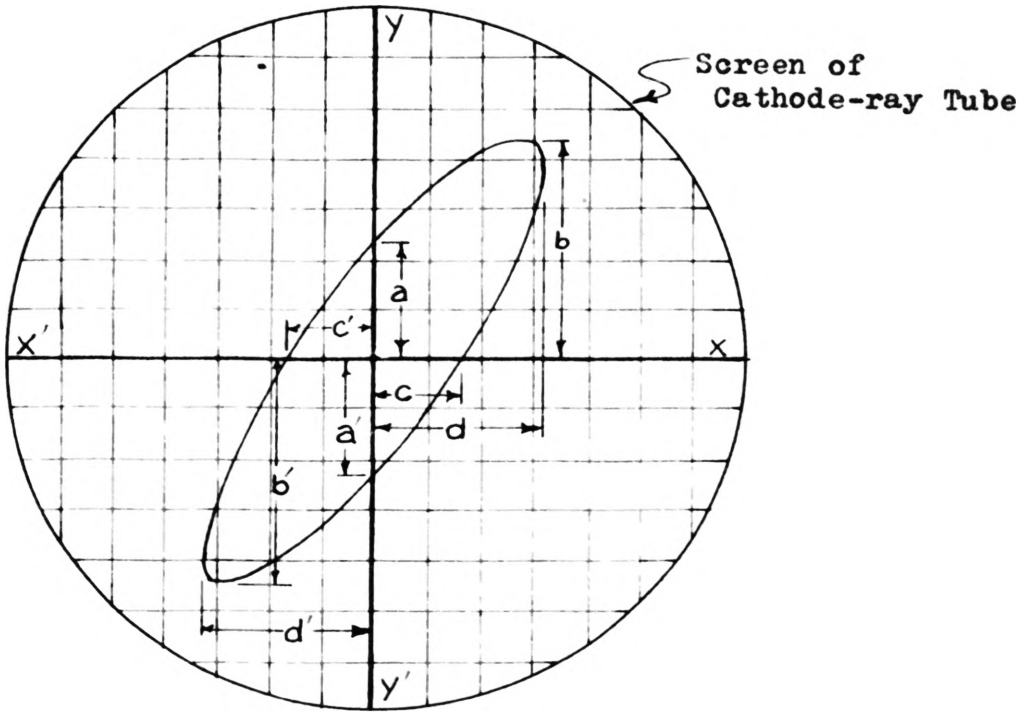

Figure 11 Example Lissajous Figure Obtained On a Cathode-ray Tube

Solving equations 52 and 53 simultaneously to eliminate ωt,

$$\sin(\omega t) = y/B \quad \text{---------- Equation 54}$$

thus, $$\cos(\omega t) = (B^2 - y^2)^{\frac{1}{2}}/B \quad \text{---------- Equation 55}$$

Expanding equation 53,

$$x/A = \sin(\omega t)\cos\phi - \cos(\omega t)\sin\phi \quad \text{---- Equation 56}$$

Substituting equations 54 and 55 into equation 56,

$$(x/A - y\cos\phi/B) = -(B^2 - y^2)^{\frac{1}{2}}\sin\phi/B$$

$$\frac{x^2}{A^2} - \frac{2xy}{AB}\cos\phi + \frac{y^2}{B^2}\cos^2\phi = \sin^2\phi - \frac{y^2}{B^2}\sin^2\phi$$

$$\frac{x^2}{A^2} - \frac{2xy}{AB}\cos\phi + \frac{y^2}{B^2} = \sin^2\phi \quad \text{------- Equation 57}$$

Equation 57 is the equation of an ellipse, the position of which is a function of the phase angle ϕ. From equation 57, let x take on the value of zero, which is y-intercept, the equation becomes

$$y^2/B^2 = \sin^2\phi$$

or $$\phi = \sin^{-1}(y/B) \quad \text{---------- Equation 58}$$

Referring to the example in figure 11:

when $x = 0$, $y = a = a'$

and $B = b = b'$

Thus, $$\phi = \sin^{-1}(a/b)$$

$$= \sin^{-1}(a'/b')$$

or $$\phi = \sin^{-1}\left(\frac{a + a'}{b + b'}\right)$$

Similarly, $x^2/A^2 = \sin^2\phi$

$$\phi = \sin^{-1}(x/A) \quad \text{---------- Equation 59}$$

$$\phi = \sin^{-1}(c/d) = \sin^{-1}(c'/d')$$

or $$\phi = \sin^{-1}\left(\frac{c + c'}{d + d'}\right)$$

Applying either equation 58 or 59 to a Lissajuous figure obtained on an oscilloscope, the phase angle between the two voltages applied to the deflection plates can be determined.

This method of determining the phase angle was used to spot check the phase angles calculated by the previously described method: e.g.

For the case of a phase difference of 90° between the two applied voltages, equation 57 reduced to the following form is;

$$x^2/A^2 + y^2/B^2 = 1 \quad \text{- - - - - - - - - - - - - - -} \quad \text{Equation 60}$$

With the dial of the phase shifter set to the 90° phase angle position, the resulting figure on the screen of the oscilloscope shows an ellipse which is symmetrical about both x- and y-axes. Therefore, this satisfies equation 60 which is also an equation of an ellipse which is symmetrical about both axes.

Similarly, when the dial was set to the 0° phase angle position, the resulting figure on the screen of the oscilloscope was a straight line satisfying the following relationship;

$$x = (A/B)y \quad \text{- - - - - - - - - - - - - - - - - - -} \quad \text{Equation 61}$$

Equation 61 is obtained by substituting $\phi = 0^{\circ}$ in equation 57.

It should be noted that determining phase angles by this method may not offer the desired high accuracy due to difficulty in reading the intercept values on the screen; however, phase angles of 90 degree multiples are readily determined.

Balancer

The 100 K potentiometer shown in figure 7 is called "Balancer" because of the nature of its function in the modeling circuit.

Calibration of the balancer was somewhat simpler than that of the phase shifter, and was made for three different voltage outputs, 2, 4,

and 6 volts, from the signal generator.

The leads connected to INPUT B, figure 7, were connected to the vertical deflection plates of the oscilloscope. As the balancer dial was set to various values, the corresponding peak to peak voltages appeared on the screen of the oscilloscope and were recorded as shown in Table 2. These values were plotted to indicate the relationship between the balancer dial settings and amplitude of the peak to peak voltage as shown in figure 12. Figure 13 is a "simplified calibration chart of the balancer" based on the curves shown in figure 12.

OPERATING PROCEDURE

Figure 14 shows the general laboratory setup of the equipment as used in these model experiments. All the leads were connected to the equipment according to the circuit diagram shown in figure 7.

The distance between the transmitting and receiving coils was adjusted to simulate a desired separation. Then the depth from the plane of the coils to the conductor model was set according to the linear scale factor being used and a model conductor was placed on the specimen stand in such a manner that its center coincides with that of the stand as shown in figure 6.

For the frequency 500 cycles per second being used for these experiments, the 0-100 cycles per second selector of the signal generator was set to give 50 cycles per second with the multiplier set at 10 times. The desired output voltage from the signal generator is secured by setting the LOAD switch to "internal". The ATTENUATOR was then set to the nearest full scale value to the desired output and the OUTPUT control was adjusted to give the desired output as indicated on the meter scale of the signal generator.

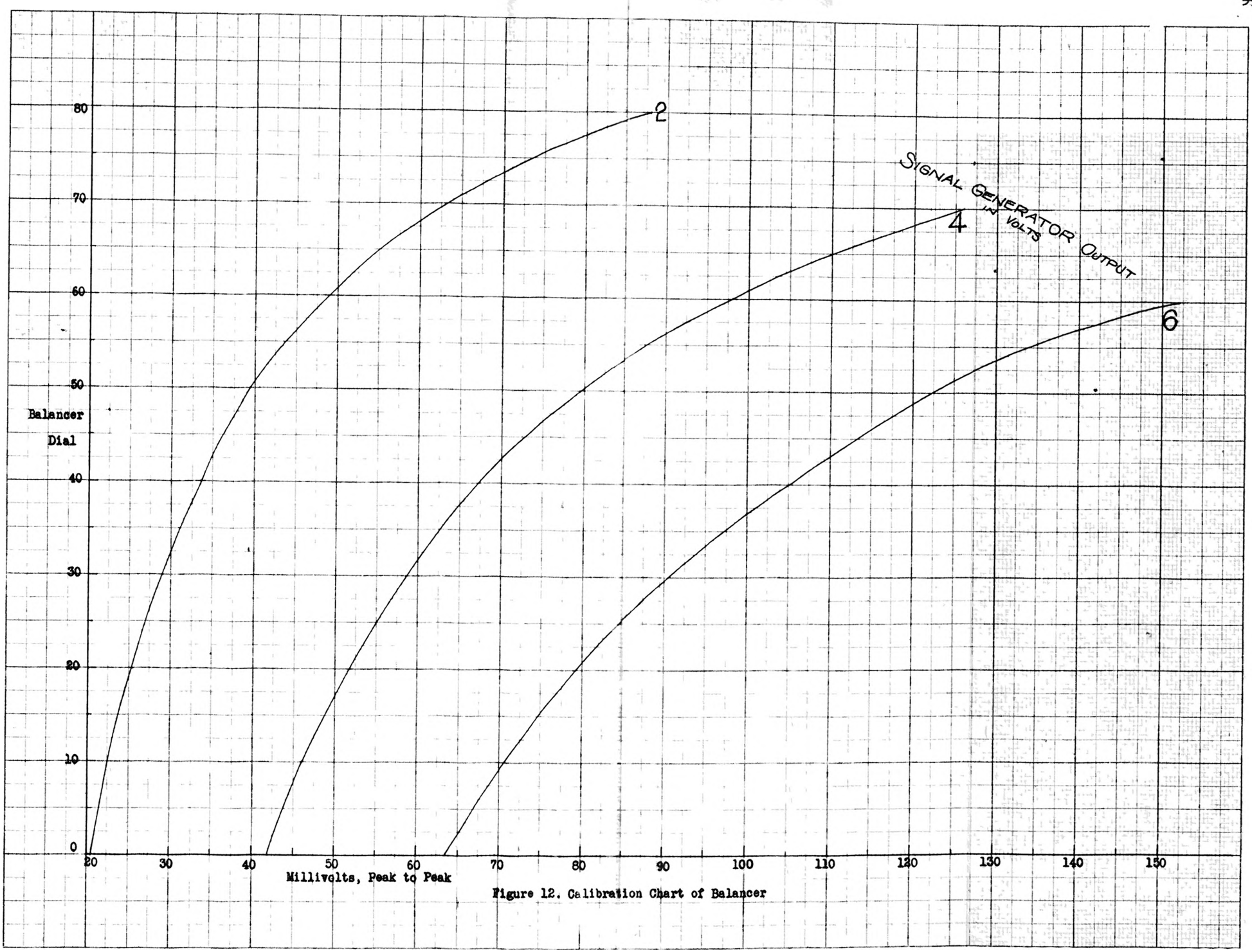

Figure 12. Calibration Chart of Balancer

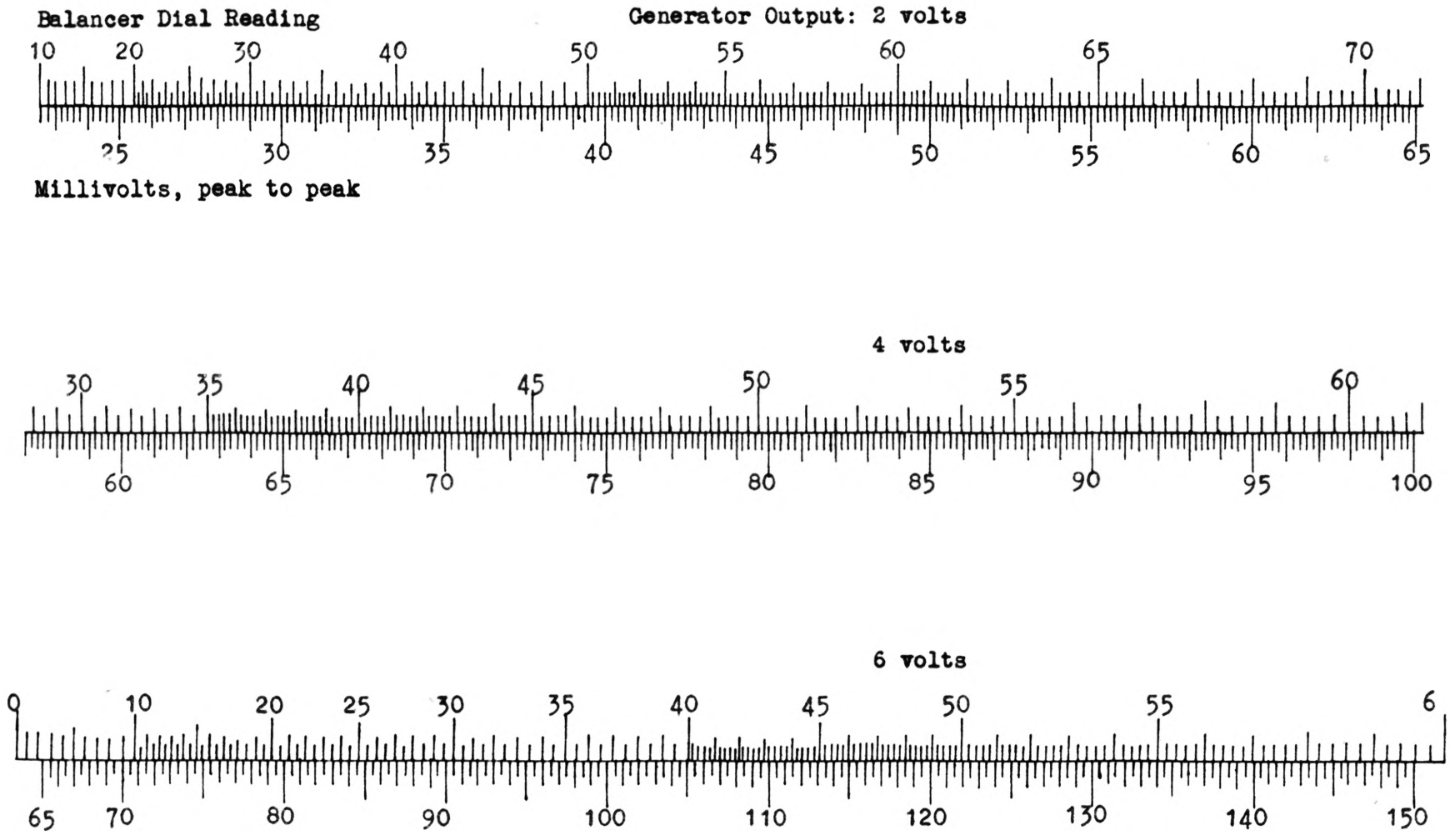

Figure 13. Simplified Calibration Chart of Balancer

The preamplifier was operated with the voltage gain control at 100 times. The high and low frequency response selectors were set at 10 kc and 80 cycles per second, respectively. The experiments were conducted with the fixed phaser selector, ϕ_s, in the circuit (or ON) and the phase shifter selector, ϕ_a, in the "OFF" position which switches the fixed resistors out of the circuit as shown in figure 15. It should be noted that the switch, ϕ_a, may be set on "ON" position when an additional phase angle is required to obtain the null.

The triggering mode selector of the cathode-ray oscilloscope was set to "automatic". The trigger slope control was on "+ internal" and the horizontal display control on "external sweep". The vertical amplitude on the oscilloscope was the sum of the amplified receiver signal and the balancing voltages from the phase shifter-balancer circuit.

With the power switch of the amplifier turned "ON" the phase shifter and balancer were adjusted until the null (a straight horizontal line) was indicated on the screen of the oscilloscope as shown in figure 16.

For the null position, the negative of the balancing voltage was exactly equal in amplitude and phase to the receiver signal. Therefore, the readings on the phase shifter and the balancer dial were a measure of phase and amplitude of the receiver signal.

RESULTS AND DISCUSSION

Several experimental curves of conductor models having different conductivities were obtained using the model study equipment so that the operating conditions and experimental techniques could be demonstrated. It should, however, be mentioned that no attempt has been made to conduct any extensive model experiment as it is beyond the scope of this research.

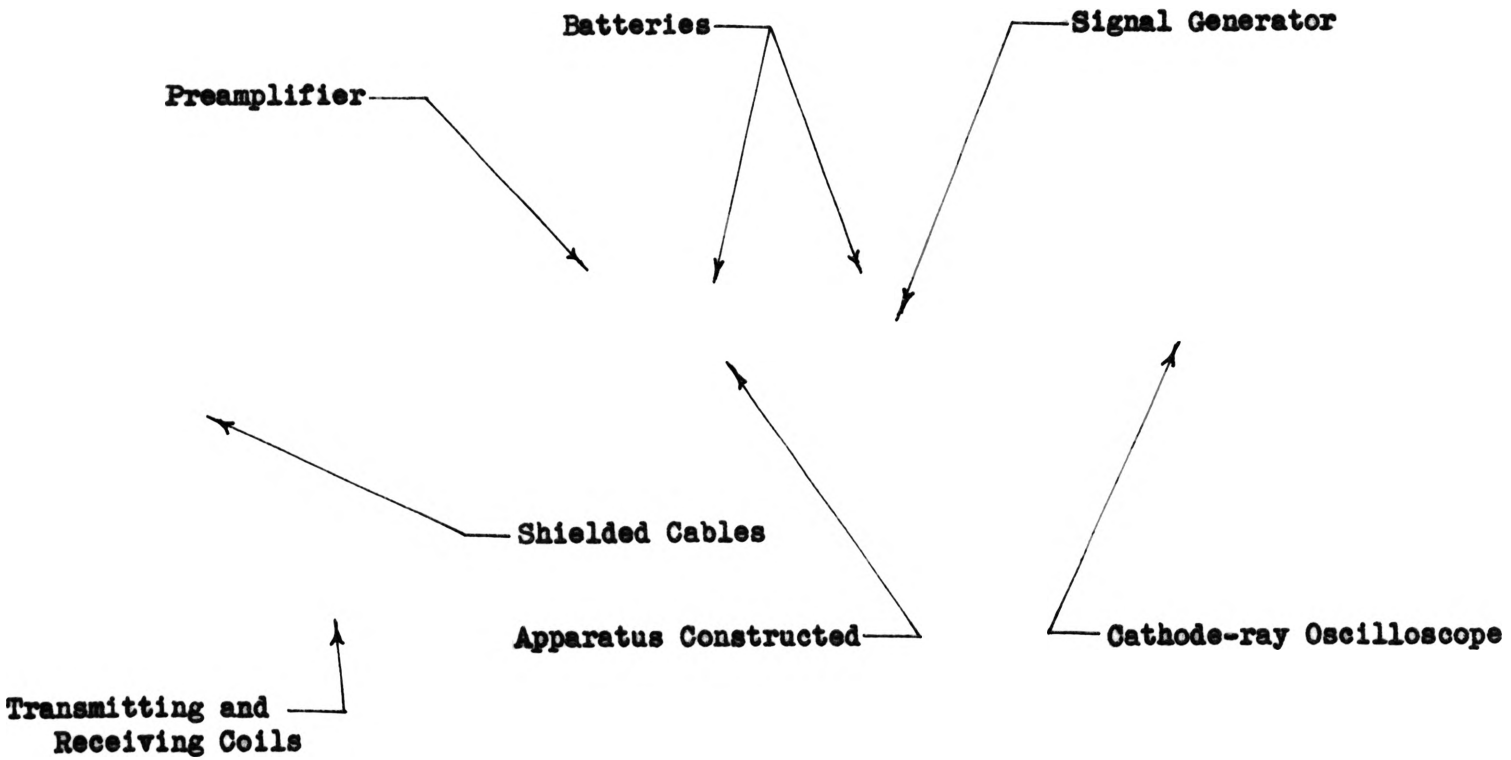
Batteries
Signal Generator
Preamplifier
Shielded Cables
Apparatus Constructed
Cathode-ray Oscilloscope
Transmitting and
Receiving Coils

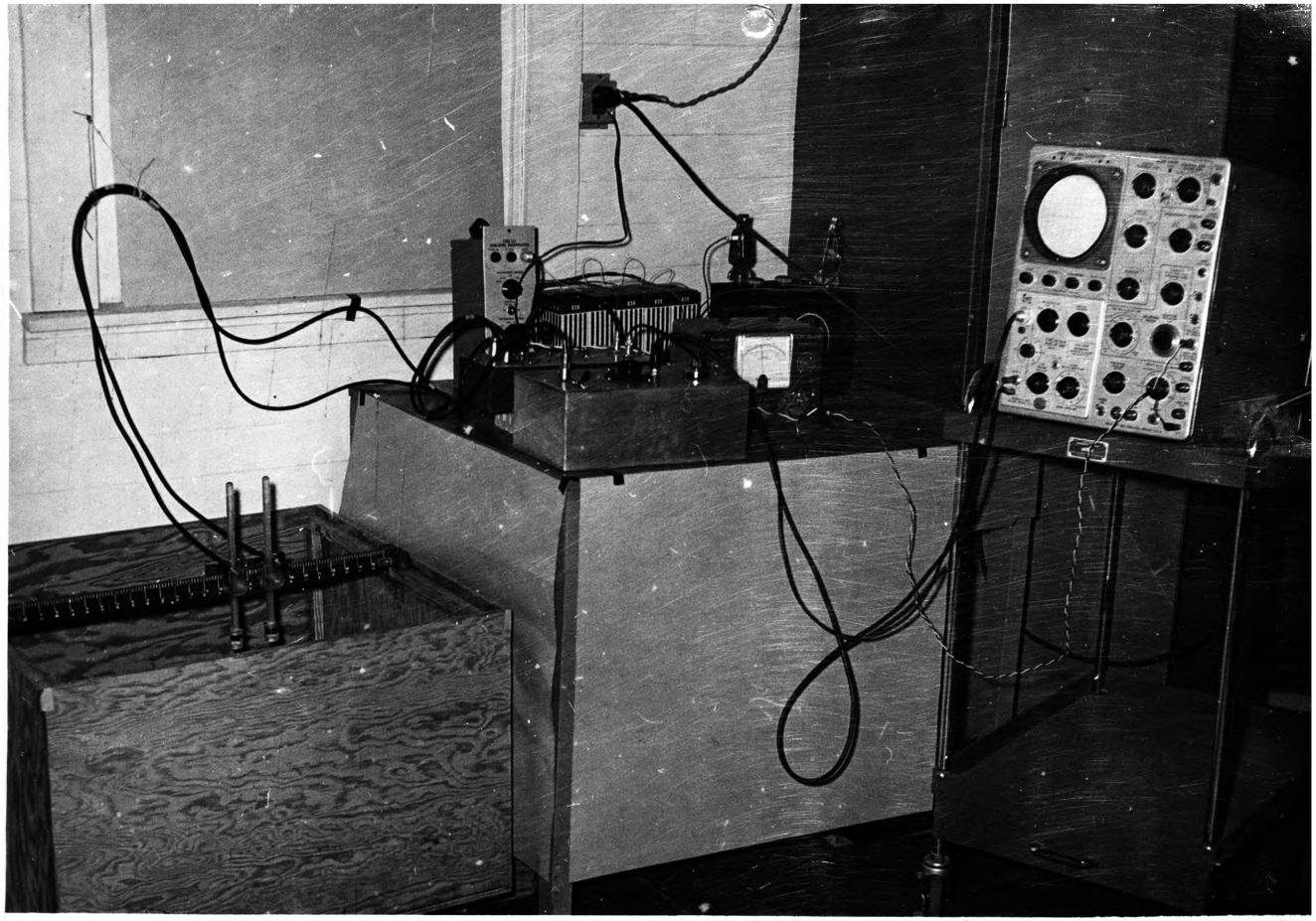

Figure 14. General Laboratory Setup of the Model Study Equipment

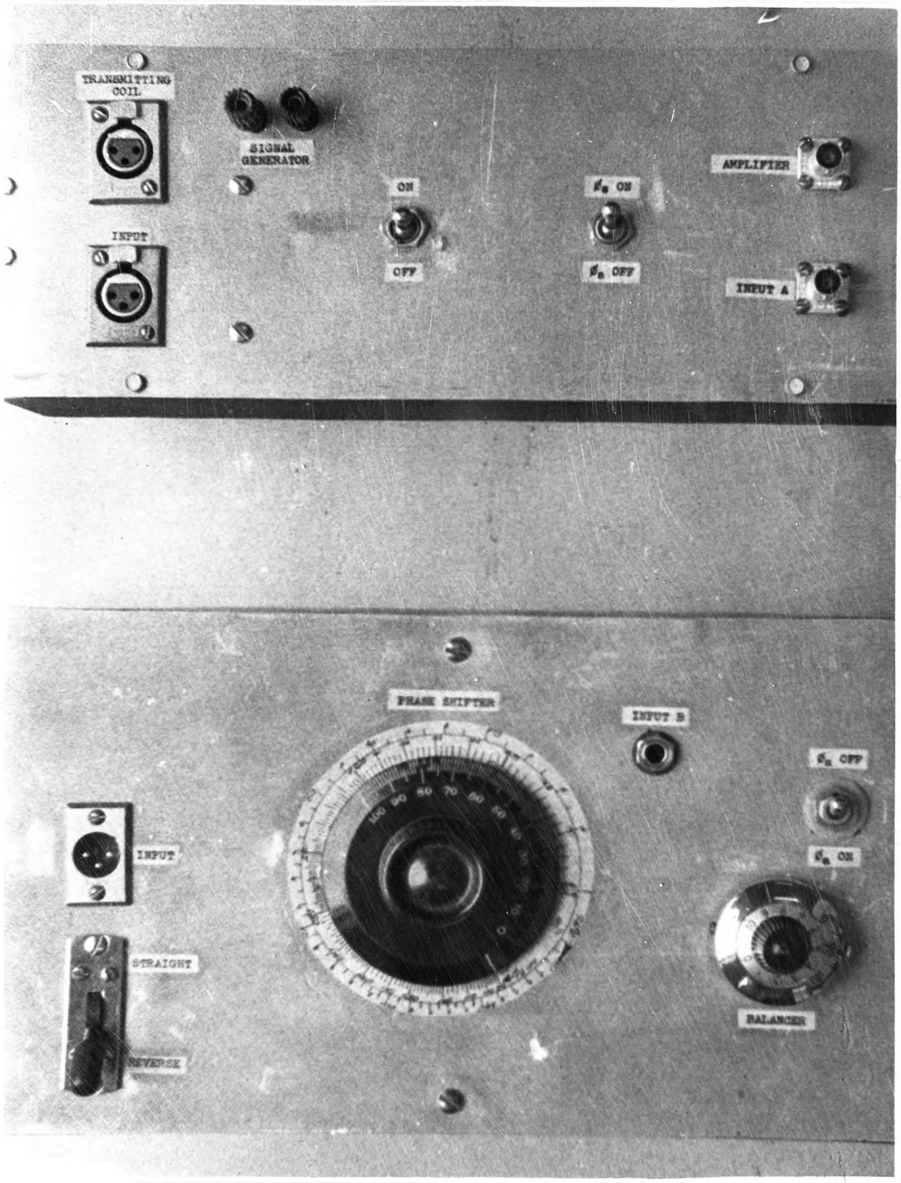

Figure 15. Apparatus Constructed for Use in the Model System

(a) INPUT A

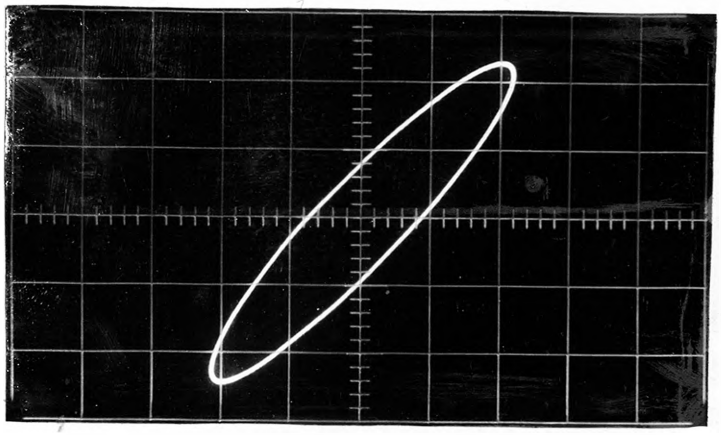

(b) INPUT A-B

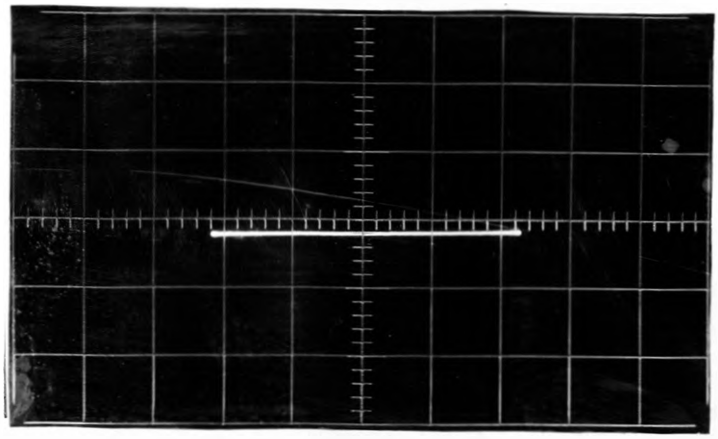

(c) INPUT B

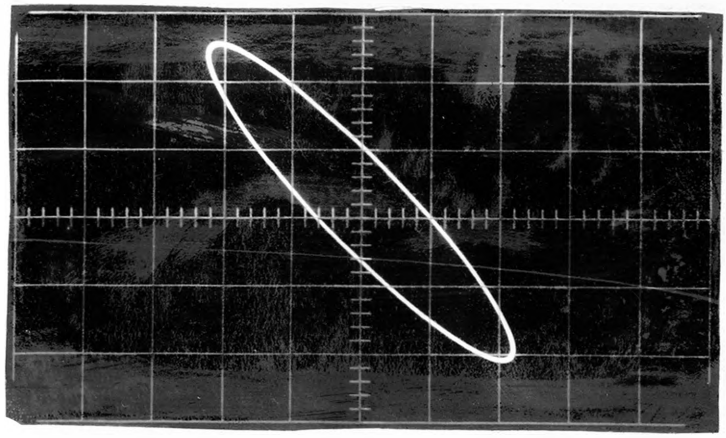

Figure 16. Example "Lissajous Figures" on an Oscilloscope Showing the Null(b) when Input A and Input B are mixed.

Readings of phase angles and balancer at the nulls on the oscilloscope were made at successive stations, $\frac{1}{2}$ inch apart, along the line of traverse. The phase angles are expressed as relative changes in phase with respect to the normal background. Amplitudes are given as the ratio of receiver to normal background amplitude. These expressions permit the results to be applied directly to interpretation of field examples.

Tables 3, 4, 5, 6 and 7 show data and results in terms of relative phase angle and amplitude ratio for various types of models. Samples showing the calculations involved in obtaining the relative phase angle and amplitude ratio showing in Table 3 are given in the Appendix. The response curves shown in figures 17, 18, 19, 20 and 22 were obtained by experiment using models of various resistivity values.

The conductor model used for figure 17 was a copper plate, 4" x 4" x 3/16", surrounded by the air and having a scaled resistivity approximating those of magnetite and specularite when a frequency of 1000 cycles per second was used in the full scale system.

From equation 47,

$$S^2 = \frac{f_m \rho_o}{f_o \rho_m} \qquad \text{Equation 62}$$

where, f_m = 500 cycles per second

S = 500

f_o = 1000 cycles per second

Substituting these values into equation 62,

$$(500)^2 = \frac{(500)\rho_o}{(1000)\rho_m}$$

$$\rho_o = 0.5 \times 10^{+6} \rho_m \qquad \text{Equation 63}$$

Substituting the resistivity value for the copper plate, 1.72×10^{-6} ohm-cm, into equation 63, the resistivity value in the full scale system

was 0.86 ohm-cm which approximates that of magnetite and specularite. The figure shows a zone of high positive amplitude ratio and negligible change in phase angle above the center of the conductor. It is seen that two zones of high negative amplitude ratio and high relative phase angles are almost symmetrical about the center line of conductor and located above the edges.

The conductor model used in the experiment shown in figure 18 was an aluminum plate, 4" x 4" x 3/16", which has a scaled resistivity approximating that of marcasite. The figure shows that the curve for the amplitude ratio is almost identical with that for the copper plate, but a greater negative relative change in phase angle occured above the center and greater positive relative phase angle above the edges of the conductor.

Figure 19 shows a response curve for a brass plate, 4" x 4" x 1/32", having a scaled resistivity approximating that a sphalerite. There is a zone of greater negative relative phase angle as compared with the cases for the copper and aluminum plates; however, there is no significant change in amplitude ratio.

Figure 20 shows the response curve for a steel plate, 4" x 4" x 1/16", having a scaled resistivity which approximates that of pyrolusite. Very high positive amplitude ratio occured above the center of the conductor and two relatively high negative zones above the points about 1 inch outside the edges. It should be noted that the shape of the response curve for relative phase angle is inverted to those mentioned previously.

A faulted bed of infinite extent in one direction was assimulated by an iron plate 12" x 3" x $\frac{1}{4}$" as shown in figure 21. The conductor

model has a scaled resistivity approximating that of pyrrhotite. It is noted that the maximum positive peaks are located approximately 3 times as far from the model edge as the maximum peaks.

CONCLUSIONS AND RECOMMENDATIONS

The author and his advisor feel that the equipment described in this thesis is suitable for model studies of electromagnetic exploration techniques. By the construction of the models in the laboratory, the geology of the earth indicated by the field measurements may be evaluated.

The response curves of the model experiment were expressed as the ratio of the magnetic field at the receiver to the source field at the transmitter. Therefore, the results obtained from the model experiment can be directly compared to those obtained from the field conditions.

It should be mentioned that by properly shielding all the leads, etc. the effect due to noise derived from the surrounding medium such as from the local radio transmitter, commercial power lines, etc. was not serious; however, it could be eliminated by placing the transmitter-receiver unit, the conductor model and the test apparatus in a shielded room.

An extensive study of the electromagnetic response of various kinds and shapes of materials of models which will simulate any geologic features desired remains to be carried out by the use of the model study equipment.

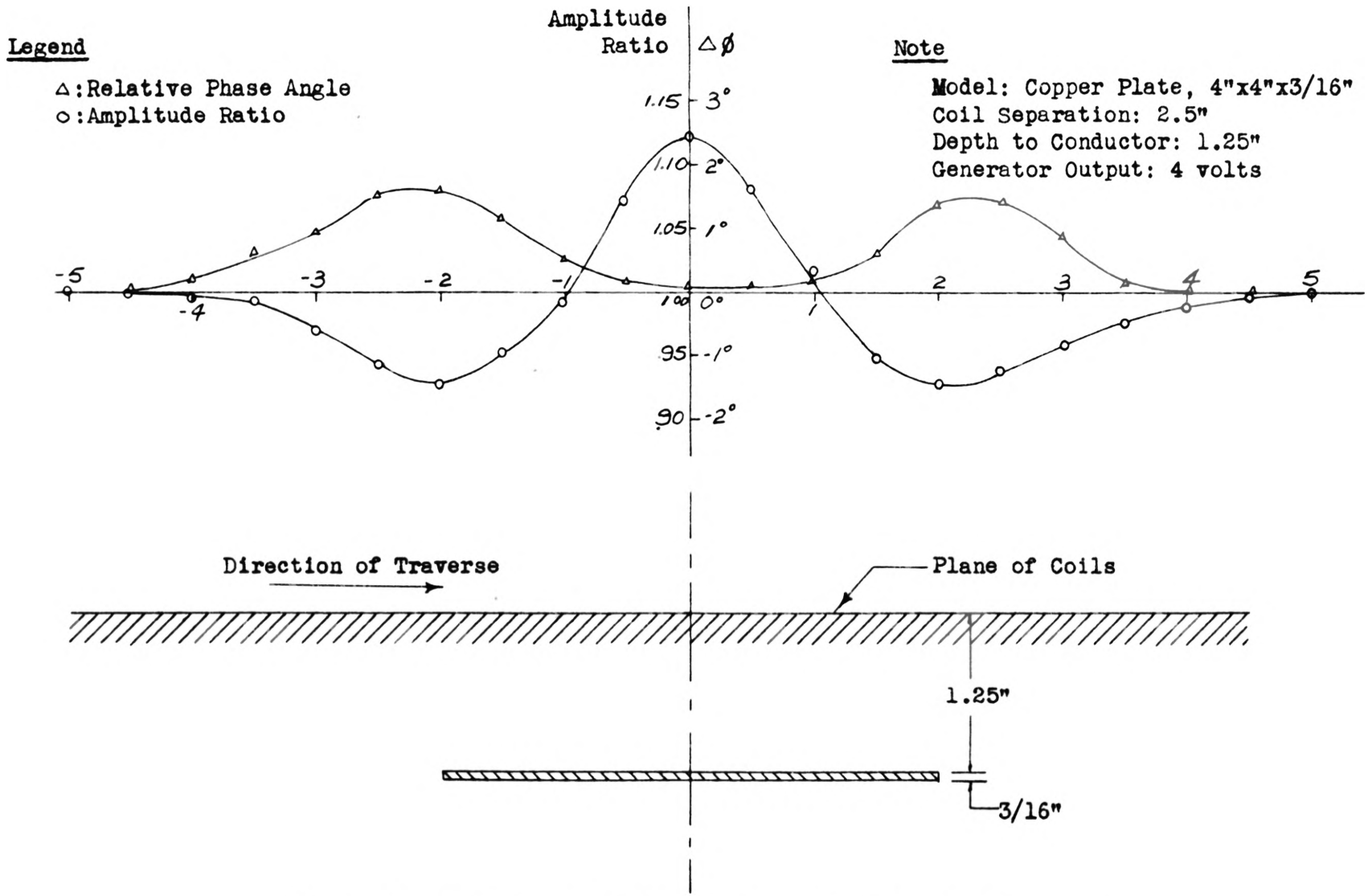

Figure 17. Horizontal Profile Showing the Amplitude Ratio and Relative Phase Angle of a Copper Plate

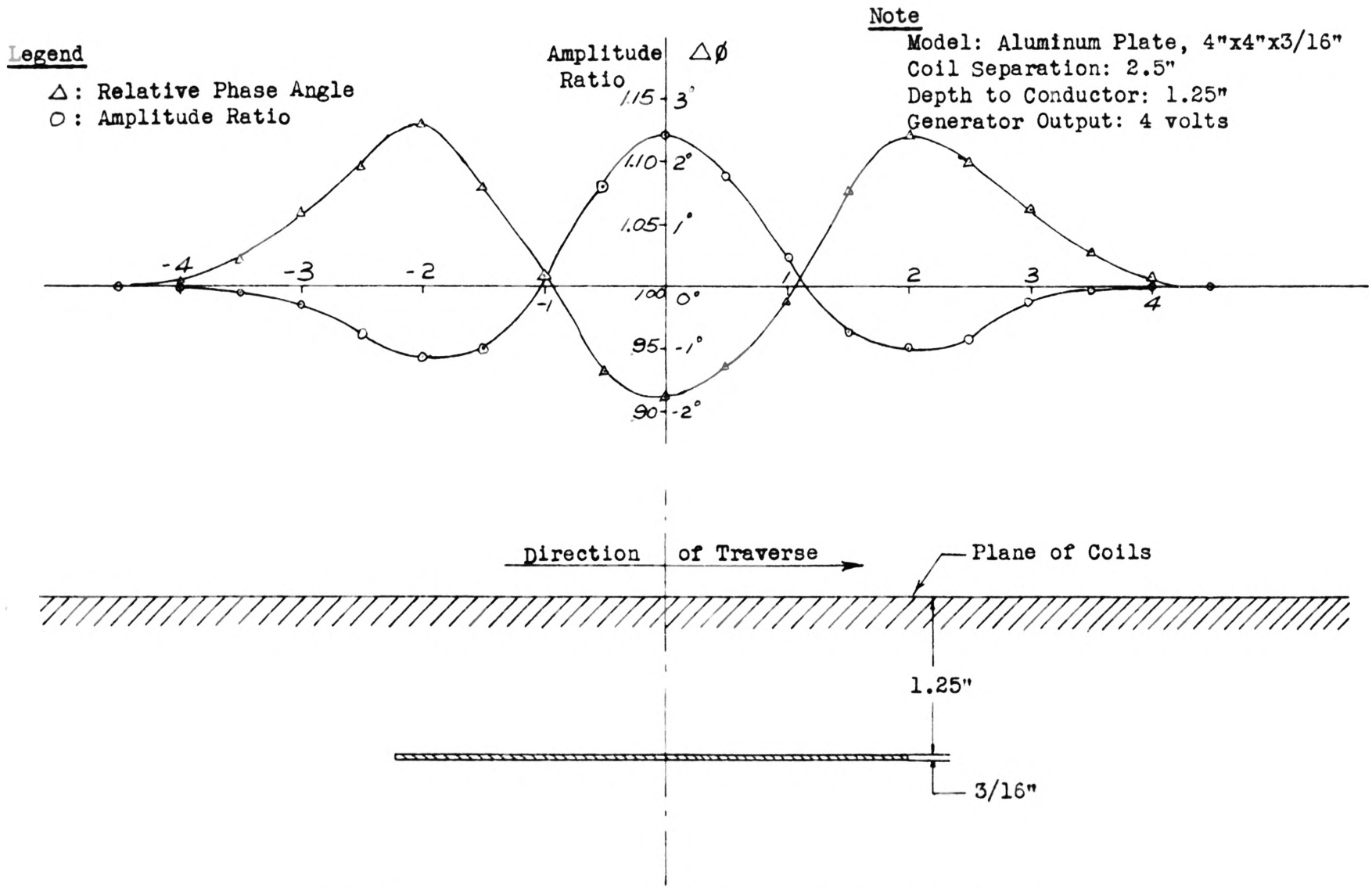

Figure 18. Horizontal Profile Showing the Amplitude Ratio and Relative Phase Angle of an Aluminum Plate

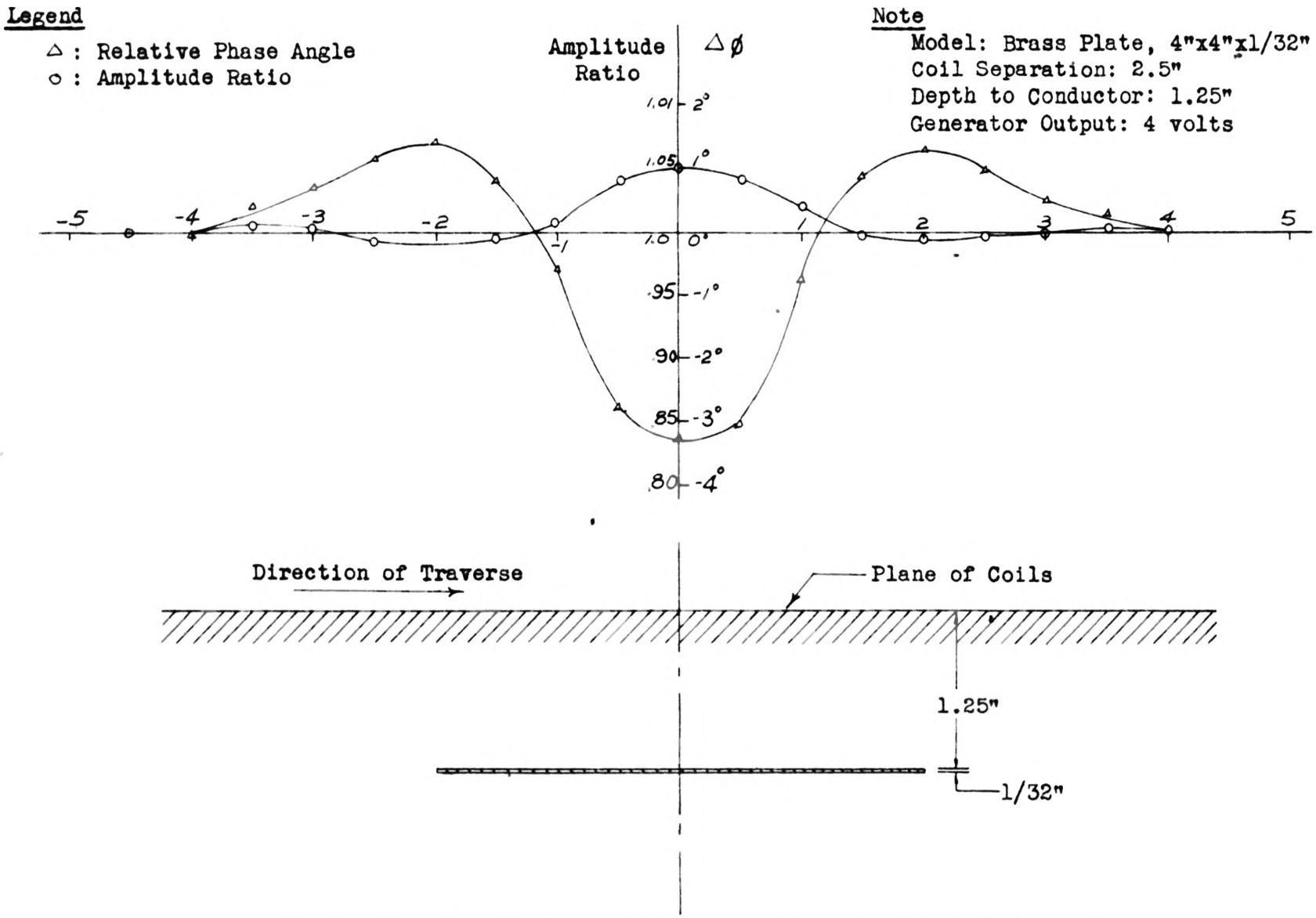

Figure 19. Horizontal Profile Showing the Amplitude Ratio and Relative Phase Angle of a Brass Plate

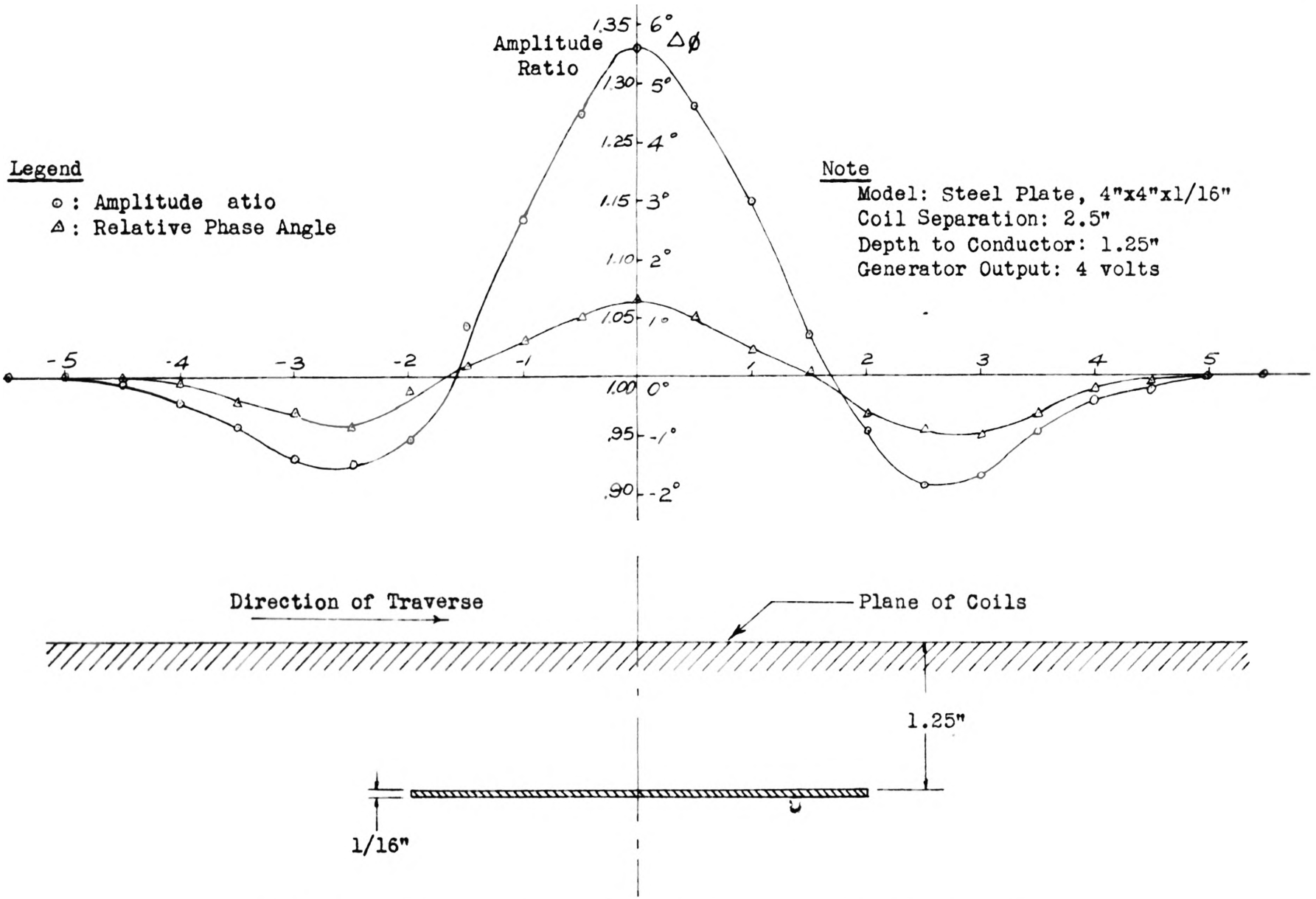

Figure 20. Horizontal Profile Showing the Amplitude Ratio and Relative Phase Angle of a Steel Plate

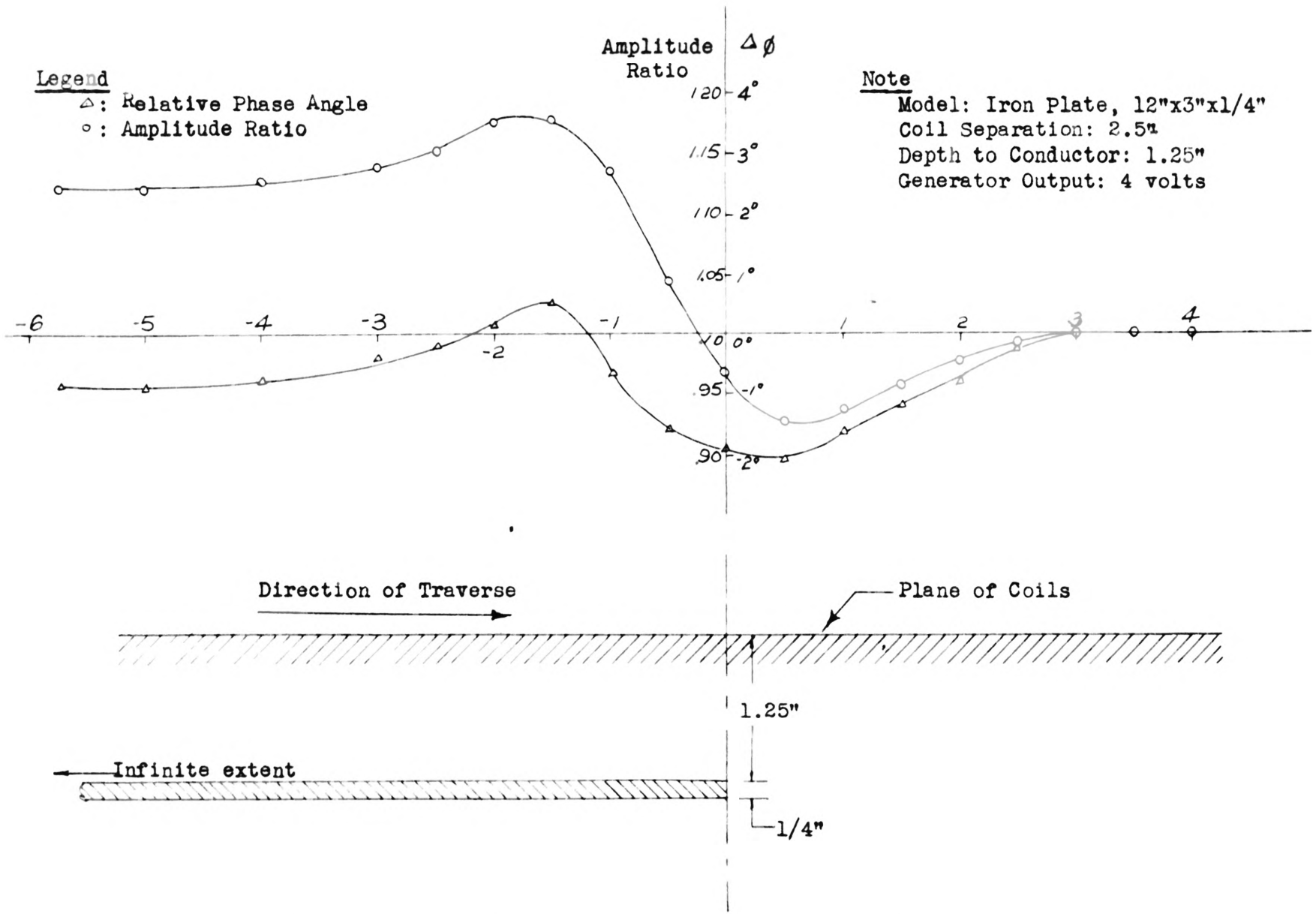

Figure 21. Horizontal Profile Showing the Amplitude Ratio and Relative Phase Angle of an Iron Plate

APPENDIX

SAMPLE CALCULATION

Table 3 is reduced for the purpose of illustration as follows:

Column: I	II	III	IV	V	VI
Traverse	ϕ in degrees	Balancer	Balancer in mv	Amplitude Ratio	$\Delta\phi$ in degrees
Free space	162.7	44.8	72.4	1.00	0
---	---	---	---	---	---
-3.0	163.6	42.8	70.1	.970	+.9
---	---	---	---	---	---

Column I, II, and III represent data obtained from a model traverse. The negative sign in the traverse denotes that the center of the coils was located to the left of the "zero" marked on the span of coil support.

The values in the column III which are dial readings of the balancer were converted to millivolts, peak to peak, in column IV by using the simplified calibration chart of the balancer given in figure 13. The values in the column are the receiver voltages amplified 100 times.

Column V which shows the amplitude ratio was calculated by dividing the balancer value in millivolts by that obtained for free space or normal background; i.e.

at traverse station, -3 --- Amplitude ratio = 70.1/72.4

= .97

Column VI indicates the relative phase angle at various traverse stations as obtained by subtracting the phase angle at free space from the phase angles at various traverse stations; i.e.

at traverse station, -3 ---$\Delta\phi = 163.6^\circ - 162.7^\circ$

$= +.9^\circ$

Dial Calibrations of Phase Shifter

Table 1

ϕ	$\cot\left(\frac{180^\circ - \phi}{2}\right)$	Rϕ	Calibration Dial
90°	1	1.10	20.0
100	1.192	1.31	23.3
110	1.428	1.57	28.2
115	1.597	1.76	31.2
120	1.732	1.905	34.3
125	1.921	2.11	38.2
130	2.145	2.36	42.8
125	2.414	2.66	48.2
140	2.746	3.02	55.0
141	2.824	3.11	56.6
142	2.904	3.20	58.2
143	2.989	3.29	60.0
144	3.078	3.38	61.8
145	3.172	3.48	63.5
146	3.271	3.60	65.3
147	3.376	3.71	67.6
148	3.487	3.82	70.0
149	3.606	3.97	72.2
150	3.732	4.10	74.4
151	3.867	4.25	77.3
152	4.011	4.41	80.2
153	4.165	4.58	83.3
154	4.332	4.77	86.5
155	4.511	4.96	90.0
156	4.705	5.17	93.5
157	4.915	4.31	98.0
158	5.145	5.65	102.5
159	5.396	5.93	107.5
160	5.671	6.23	113.2
161	5.976	6.57	119.4
162	6.314	6.94	126.1
163	6.691	7.36	134.0
164	7.115	7.83	142.5
165.0	7.596	8.36	152.0
165.2	7.700	8.47	153.5
165.4	7.806	8.59	155.7
165.6	7.916	8.71	158.0
165.8	8.029	8.83	160.4
166.0	8.144	8.95	162.8
166.2	8.264	9.09	165.2
166.4	8.386	9.22	167.7
166.6	8.513	9.36	170.1

Dial Calibrations of Phase Shifter (Cont.)

ϕ	$\cot\left(\frac{180^\circ - \phi}{2}\right)$	$R\phi$	Calibration Dial	
166.8	8.643	9.52	172.6	
167.0	8.777	9.65	175.2	
167.2	8.915	9.80	178.0	
167.4	9.058	9.96	181.0	
167.6	9.205	10.13	2.	After ϕ_a on
167.8	9.357	10.29	5.2	
168.0	9.514	10.47	8.3	
168.2	9.677	10.65	11.5	
168.4	9.845	10.83	15.	
168.6	10.019	11.02	18.3	
168.8	10.199	11.22	22.0	
169.0	10.385	11.42	25.6	
169.2	10.579	11.64	29.5	
169.4	10.780	11.86	33.7	
169.6	10.988	12.09	37.9	
169.8	11.205	12.33	42.3	
170.0	11.430	12.57	46.8	
170.2	11.664	12.83	51.5	
170.4	11.909	13.10	56.3	
170.6	12.207	13.43	62.3	
170.8	12.429	13.67	67.2	
171.0	12.706	13.98	72.0	
171.2	12.996	14.30	77.5	
171.4	13.300	14.63	84.2	
171.6	13.617	14.98	90.1	
171.8	13.951	15.35	97.0	
172.0	14.301	15.73	100.4	
172.2	14.669	16.13	111.0	
172.4	15.056	16.51	119.0	
172.6	15.464	17.01	127.0	
172.8	15.895	17.49	136.0	
173.0	16.350	17.99	145.0	
173.2	16.832	18.52	155.0	
173.4	17.343	19.08	165.5	
173.6	17.866	19.65	176.0	

Dial Calibration of Balancer

Table 2

Dial Readings	At Gen output = 2v Corresponding Value in mv, peak to peak	At Gen output = 4v Corresponding Value in mv, peak to peak	At Gen output = 6v Corresponding Value in mv, peak to peak
0	20.5	41.8	63.3
10	22.5	46.0	70.8
20	25.5	51.8	79.2
30	29.0	58.5	90.5
40	33.5	67.4	105
50	39.4	79.5	122
60	48.8	98.0	152
70	63.2	126.0	194
80	88.0	174.0	225
90	150.0	302.0	464
100	520.0	1,210	1,600

Data for Traverse Using Copper Plate Model

Table 3

Traverse	∅ in degree	Balancer Dial	Balancer in mv	Amplitude Ratio	∅ in degree
Free Space	162.7	44.8	72.4	1.000	0
- 5.0	162.7	44.8	72.4	1.000	0
- 4.5	162.8	44.7	72.3	0.999	+ 0.1
- 4.0	162.9	44.5	72.1	0.996	+ 0.2
- 3.5	163.3	44.3	71.8	0.993	+ 0.6
- 3.0	163.6	42.8	70.1	0.970	+ 0.9
- 2.5	164.2	40.9	68.1	0.941	+ 1.5
- 2.0	164.3	39.8	67.1	0.927	+ 1.6
- 1.5	163.9	41.5	68.8	0.951	+ 1.2
- 1.0	163.2	44.4	72.0	0.995	+ 0.5
- 0.5	162.9	48.6	77.5	1.070	+ 0.2
0	162.8	51.0	81.1	1.120	+ 0.1
0.5	162.8	49.0	78.1	1.080	+ 0.1
1.0	162.9	45.6	73.5	1.015	+ 0.2
1.5	163.3	41.2	68.5	0.946	+ 0.6
2.0	164.1	39.8	67.1	0.927	+ 1.4
2.5	164.1	40.3	67.6	0.935	+ 1.4
3.0	163.6	42.0	69.3	0.958	+ 0.9
3.5	162.8	43.2	76.5	0.975	+ 0.1
4.0	162.7	44.0	71.5	0.988	0
4.5	162.7	44.6	72.2	0.997	0
5.0	162.7	44.8	72.4	1.000	0

Model: Copper Plate, 4" x 4" x 3/16"
Generator Output: 4 volt rms
Coil Separation (S): 2.5 inch
Depth to Conductor: 1.25 inch

Date for Traverse Using Aluminum Plate Model

Table 4

Traverse	∅ in degree	Amplitude Dial	Amplitude in mv	Amplitude Ratio	∅ in degree
Free Space	161.9	49.0	78.1	1.000	0
- 4.5	161.9	49.0	78.1	1.000	0
- 4.0	162.0	49.0	78.1	1.000	+ 0.1
- 3.5	162.3	48.6	77.5	0.994	+ 0.4
- 3.0	163.1	48.2	76.8	0.985	+ 1.2
- 2.5	163.8	46.8	75.0	0.961	+ 1.9
- 2.0	164.5	45.7	73.6	0.943	+ 2.6
- 1.5	163.5	46.2	74.2	0.950	+ 1.6
- 1.0	162.1	49.3	78.6	1.009	+ 0.2
- 0.5	160.5	52.9	84.2	1.008	- 1.4
0	160.1	54.9	87.4	1.120	- 1.8
0.5	160.6	53.4	84.9	1.088	- 1.3
1.0	161.6	50.0	79.7	1.020	- 0.3
1.5	163.4	46.8	75.0	0.961	+ 1.5
2.0	164.3	46.2	74.2	0.950	+ 2.4
2.5	163.9	46.4	74.5	0.955	+ 2.0
3.0	163.1	48.1	76.8	0.985	+ 1.2
3.5	162.4	48.9	78.0	0.998	+ 0.5
4.0	162.0	49.0	78.1	1.000	+ 0.1
4.5	161.9	49.0	78.1	1.000	0

Model: Aluminum Plate, 4" x 4" x 3/16"
Generator Output: 4 volt rms
Coil Spacing (S): 2.5 inch
Depth (d): 1.25 inch

Date for Traverse Using Brass Plate Model

Table 5

Traverse	∅ in degree	Amplitude Dial	Amplitude in mv	Amplitude Ratio	∅ in degree
Free Space	161.9	49.0	78.1	1.000	0
- 4.5	161.9	49.0	78.1	1.000	0
- 4.0	161.9	49.1	78.2	1.001	0
- 3.5	162.3	49.2	78.4	1.003	+ 0.4
- 3.0	162.6	49.2	78.4	1.003	+ 0.7
- 2.5	163.0	48.6	77.5	0.992	+ 1.1
- 2.0	163.8	48.7	77.6	0.995	+ 1.9
- 1.5	163.2	48.8	77.8	0.996	+ 1.3
- 1.0	161.3	49.4	78.7	1.008	- 0.6
- 0.5	159.1	50.9	81.0	1.038	- 2.8
0	157.6	51.5	81.8	1.048	- 3.3
0.5	158.8	51.0	81.1	1.040	- 3.1
1.0	161.1	49.9	79.6	1.020	- 0.8
1.5	162.8	48.9	78.0	0.998	+ 0.9
2.0	163.2	48.8	77.8	0.996	+ 1.3
2.5	162.9	48.9	78.0	0.998	+ 1.0
3.0	162.4	49.0	78.1	1.000	+ 0.5
3.5	162.0	49.2	78.3	1.002	+ 0.3
4.0	161.9	49.1	78.2	1.001	0
4.5	161.9	49.0	78.1	1.000	0

Model: Brass Plate, 4" x 4" x 1/32"
Generator Output: 4 volt rms
Coil Spacing (S): 2.5 inch
Depth (d): 1.25 inch

Data for Traverse Using Steel Plate Model

Table 6

Traverse	ø in degree	Amplitude Dial	Amplitude in mv	Amplitude Ratio	ø in degree
Free Space	162.8	44.8	72.4	1.000	0
- 5.0	162.8	44.8	72.4	1.000	0
- 4.5	162.8	44.4	72.0	0.995	0
- 4.0	162.7	43.4	70.8	0.978	- 0.1
- 3.5	162.4	42.1	69.3	0.957	- 0.4
- 3.0	162.2	40.0	67.3	0.930	- 0.6
- 2.5	161.9	39.4	66.8	0.925	- 0.9
- 2.0	162.6	41.4	68.7	0.948	- 0.2
- 1.5	163.0	47.2	75.5	1.042	+ 0.2
- 1.0	163.4	51.7	82.2	1.135	+ 0.6
0.5	163.8	55.5	88.5	1.222	+ 1.0
0	164.1	56.7	90.8	1.253	+ 1.3
0.5	163.8	55.8	89.1	1.230	+ 1.0
1.0	163.3	52.4	83.3	1.150	+ 0.5
1.5	162.9	46.9	75.1	1.038	+ 0.1
2.0	162.1	41.8	69.1	0.955	- 0.7
2.5	161.9	38.5	65.8	0.909	- 0.9
3.0	161.8	39.2	66.5	0.918	- 1.0
3.5	162.0	41.8	69.1	0.955	- 0.6
4.0	162.6	43.6	71.0	0.980	- 0.2
4.5	162.7	44.0	71.5	0.987	- 0.1
5.0	162.8	44.8	72.4	1.000	0

Model: Steel Plate, 4" x 4" x 1/16"
Generator Output: 4 volts rms
Coil Separation (S): 2.5 inch
Depth (d): 1.25 inch

Data for Traverse Using Iron Plate Model

Table 7

Traverse	ϕ in degree	Amplitude Dial	Amplitude in mv	Amplitude Ratio	ϕ in degree
Free Space	162.8	43.7	71.2	1.000	0
- 5.5	161.9	50.1	79.8	1.120	- 0.9
- 5.0	161.9	50.1	79.8	1.120	- 0.9
- 4.0	162.0	50.3	80.1	1.126	- 0.8
- 3.0	162.4	51.0	81.1	1.140	- 0.4
- 2.5	162.6	51.9	81.8	1.150	- 0.2
- 2.0	162.9	52.6	83.6	1.175	+ 0.1
- 1.5	163.3	52.7	83.8	1.180	+ 0.5
- 1.0	162.1	50.8	80.8	1.135	- 0.7
- 0.5	161.2	46.3	74.3	1.044	- 1.6
0	160.9	41.6	68.9	0.968	- 1.9
0.5	160.7	38.6	65.9	0.925	- 2.1
1.0	161.2	39.3	66.0	0.936	- 1.6
1.5	161.6	40.9	68.1	0.957	- 1.2
2.0	162.0	42.2	69.5	0.977	- 0.8
2.5	162.6	43.2	70.6	0.993	- 0.2
3.0	162.8	43.6	71.1	0.999	0
3.5	162.8	43.7	71.2	1.000	0

Model: Iron Plate, 12" x 3" x $\frac{1}{4}$"
Generator Output: 4 volt rms
Coil Separation (S): 2.5 inch
Depth (d): 1.25 inch

BIBLIOGRAPHY

(1) Slichter, L. B.: "Observed and Theoretical Electromagnetic Model Response of Conducting Spheres," A.I.M.E. Trans., Geophysical Prospecting, p. 443-459, 1932

(2) Clark, A. R. and Mungal, A. G.: "Scale Model Experiments in Electromagnetic Methods of Geophysical Exploration," Canadian Journal of Physics, Vol. 29, p. 285-293, 1951

(3) Zuschlag, Theodor: "Mapping Oil Structures by the Sundberg Method," A.I.M.E. Trans., Geophysical Prospecting, p. 144-156, 1932

(4) Hedstrom, E. H. and Parasnis, D. S.: "Some Model Experiments Relating to Electromagnetic Prospecting with Special Reference to Airborne Work," Geophysical Prospecting, Vol. 6, p. 321-341, 1958

(5) Jakosky, J. J.: Exploration Geophysics, 2nd Edition (1957), Trija Publishing Company, p. 580-631

(6) Heiland, C. A.: Geophysical Exploration, Prentice-Hall, Inc., p. 685, 1940

(7) Sinclair, George: "Theory of Models of Electromagnetic Systems," Institute of Radio Engineers Proceedings, Vol. 36, p. 1364-1370, 1948

(8) Stratton, J. A.: Electromagnetic Theory, McGraw-Hill Book Co., Inc., p. 448, 1931

References not Cited:

Hedstrom, Helmer: "Phase Measurements in Electrical Prospecting," A.I.M.E. Trans., Vol. 138, p. 456-472, 1940

Hague, B.: Alternating Current Bridge Methods, 3rd Ed. (1932), London Sir Isaac Pitman & Sons, Ltd.

Roters, Herbert C.: Electromagnetic Devices, 1st Ed. (1948), John Wiley & Sons, Inc.

Suydam, Vernon A.: Electricity and Electromagnetism, 4th Printing (1947), D. Van Nostrand Co., Inc., N. Y., p. 520-530

Wright, R.R.: Electronics, Principles and Applications, The Ronald Press Company, p. 245, 1950

VITA

Won Ho Kim, the son of Mr. and Mrs. Dae Yoon Kim, was born at Chinnampo, Korea, on October 7, 1935.

He received his elementary and secondary education at various government schools in Korea. Upon graduating from the Kyung-Bock High School in Seoul, he registered at the College of Engineering, Seoul University in 1954.

In February of 1956, he came to the United States and enrolled in the Missouri School of Mines and Metallurgy, from which he received the B. S. degree in Mining Engineering in May, 1959.

In September, 1959, he enrolled for graduate study in geophysics in the Department of Mining Engineering, Missouri School of Mines and Metallurgy, Rolla, Missouri.

He is a member of Sigma Gamma Epsilon, Sigma Xi, the Society of Exploration Geophysicists, and the American Geophysical Union.